Universität Leipzig
Fakultät für Physik und Geowissenschaften
Institut für Theoretische Physik

Master Thesis

Polymer Adsorption onto a Stripe-Patterned Surface

Momchil Ivanov
9918005

October, 2012

Referees: *Prof. Dr. Wolfhard Janke*
Prof. Dr. Ulrich Behn
Supervisors: *Prof. Dr. Wolfhard Janke*
Dipl. Phys. Monika Möddel

Contents

Nomenclature

AC Adsorbed-compact

AE Adsorbed-expanded

DC Desorbed-compact

DE Desorbed-expanded

ISAW Interacting Self Avoiding Walk

MC Monte Carlo

PERM Pruned-Enriched Rosenbluth Method

SAG Surface Attached Globule

SAW Self Avoiding Walk

Chapter 1

Introduction

The scientific and technological progress during the past century has pushed experimental and manufacturing techniques to the nano-meter scale. With the advance of experimental techniques such as the scanning tunnelling microscopy, the atomic force microscopy and optical tweezers, one is able to access and even manipulate physical objects on the atomic level [1, 2, 3, 4]. This creates the need to understand the physics on that scale in order to be able to study the processes in biological systems, to be able to create new chemical substances and to be able to engineer new materials. Proteins are essential components of the living systems as we know them on earth. The study of their interaction with surfaces such as membranes, catalysts and porous materials is important for biological research. Many functional materials include special coatings that prevent adhesion of certain substances. The deposition of a macro-molecule on a surface in a predefined conformation is a problem yet to be solved. One can, for instance, stretch molecules immersed in liquids with the help of optical tweezers [5]. There are, however, no means to force the creation of other specific conformations or to deposit them on a substrate. Understanding the physics of these systems is also an interesting undertaking because the processes are guided by the fight between entropy and energy. However, the complexity of the systems does not allow for a straightforward theoretical analysis.

An important step towards the research on polymers has been the availability of powerful computing machines due to the technological advance in recent years. These can be used to study the properties of virtual systems using sophisticated simulation techniques [6, 7, 8, 9, 10, 11, 12]. The computer models contain the most important interactions and exhibit similar transitions as the real world. This allows the study of every aspect of the system without the need to deal with the perversity of matter. One can varying every parameter at will, which is not possible in the real world. Temper-

ature, for instance, is a parameter that is hard to control and manipulate in an experiment. Moreover, the equipment used in an experiment has spatial dimensions and operating environment requirements, meaning that only a number of compatible measuring and controlling devices fit in a typical experimental setup. This gives access to only a few observables. Detecting other properties of the system might require a completely new experimental setup using other experimental methods, or might be impossible due to the lack of experimental techniques or equipment. These are, however, no limitations for a computer model. One can measure every property of the system or parts thereof during the course of an experiment (computer simulation).

Recently, the phase diagram of a non-grafted finite interacting self-avoiding walk (ISAW) near an attractive substrate has been constructed [13]. The ISAW is one of the simplest models that exist for polymers. It simulates a self-interaction between nonadjacent monomers and undergoes a collapse or coil-globule transition from a high-temperature phase to a low temperature phase, and another transition at even lower temperatures forming crystalline structures called freezing transition [14]. Adding an attractive surface introduces the adsorption transition to the system, where at low temperatures the polymer is adsorbed and at high temperature desorbed. The interplay between both attractions gives rise to the existence of different phases depending on the strength of each interaction. Phases in this work mean pseudo-phases (except otherwise mentioned), since the systems discussed have finite size. The word "pseudo" has been omitted to ease the reader. The pseudo-phases that I am referring to indicate regions on the phase diagram where the system has similar properties. Some of these pseudo-phases are believed to exist as phases in the thermodynamic sense for longer chains, others however, exist only in the specified length scales.

The goal of this work is to add attractive parallel stripes to the model and to study the effect of such stripes on the phase diagram compared to a homogeneous substrate surface. This is a simple pattern and can serve as a the basis for understanding the adsorption of polymers on substrates containing more complicated patterns. The effects of the the stripe-attraction strength on the phase diagram are being studied for two different stripe widths. The corresponding phase diagrams are constructed using both canonical and microcanonical analysis. The differences and similarities between the resulting two diagrams are discussed and analytical calculations are given where possible. The effect of the self-attraction on the phase diagram is also being discussed, as it leads to qualitatively different results and changes the set of available phases. The dependence of the phase diagram on the confinement volume is discussed as it has either minor or major influence, depending on the length scale. Additionally, the results are compared with the literature

on an equivalent off-lattice model in reference [12].

Chapter 2

The Model

2.1 Introduction

This work investigates the properties of a simple polymer system in three dimensions. The system lives on a simple cubic lattice and has only nearest neighbour interactions, i.e. only neighbouring sites can interact with each other. An interacting self-avoiding walk is used to model the polymer chain. Each point of the walk represents a monomer of the polymer, an interaction of nonadjacent monomer-monomer neighbours is used and the excluded volume constraint is modelled by the self-avoidance constraint. Two other types of constraints are introduced in the form of infinitely extended impenetrable walls: an attractive one and a steric one with no interactions whatsoever. Moreover, the attractive wall is patterned with parallel stripes whose attraction can be different from the rest of the wall. An illustration is given on Figure 2.1. The energy of the ISAW is defined as:

$$E(n_{\mathrm{s}}, n_{\mathrm{str}}, n_{\mathrm{m}}) = -\epsilon_{\mathrm{s}} n_{\mathrm{s}} - \epsilon_{\mathrm{str}} n_{\mathrm{str}} - \epsilon_{\mathrm{m}} n_{\mathrm{m}}, \tag{2.1}$$

where n_{s}, n_{str} and n_{m} are the number of monomer-surface (excluding stripes), monomer-stripes, monomer-monomer (excluding adjacent neighbours) contacts, respectively. The strength of the interactions is modelled by the parameters ϵ_{s}, ϵ_{str} and ϵ_{m}, respectively. One can use a common energy scale ϵ_{s} and rescale $\epsilon_{\mathrm{str}} = a\epsilon_{\mathrm{s}}$ and $\epsilon_{\mathrm{m}} = b\epsilon_{\mathrm{s}}$. The energy becomes

$$E(n_{\mathrm{s}}, n_{\mathrm{str}}, n_{\mathrm{m}}) = -\epsilon_{\mathrm{s}} \left(n_{\mathrm{s}} + a n_{\mathrm{str}} + b n_{\mathrm{m}}\right) \tag{2.2}$$

and this gives one the possibility to tune the strength of monomer-stripes and monomer-monomer interactions relative to the monomer-surface interaction via the parameters a and b. The case $a = b = 1$ means that all

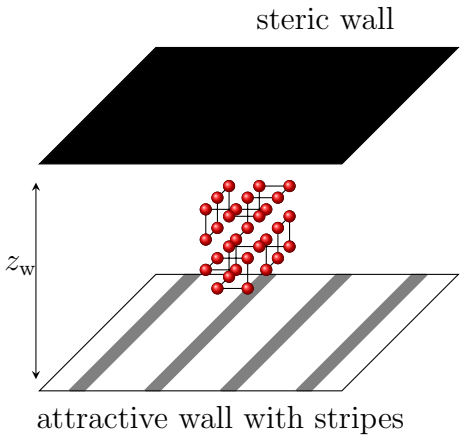

Figure 2.1: A SAW in a cavity of height z_w, where the lower wall is attractive and patterned with stripes indicated by thick grey lines, the upper wall is steric. The balls represent the monomers of the chain and the connecting line is the self-avoiding walk.

interactions have equal strength, i.e. $\epsilon_s = \epsilon_{str} = \epsilon_m$. In the following, I choose $\epsilon_s = k_B \equiv 1$.

2.2 The confinements

Two cases of confinements are considered: grafted and non-grafted. In the grafted case, one end of the ISAW is fixed on the surface of the attractive wall and the rest of the chain is allowed to move freely. In the non-grafted case, the ISAW is allowed to move freely between the two infinitely extended parallel walls. The steric wall's sole purpose is to confine the volume in which the ISAW can move. Without that last constraint the volume of the system would be infinite. This makes the number of possible positions of the free chain (chain without any possible contacts to a wall) infinite. That would make the relative number of adsorbed conformations vanish and would not allow the study of adsorption. In formulae, the probability of a conformation with (n_s, n_{str}, n_m) contacts at a temperature T and fixed parameters a and b is:

$$p(n_s, n_{str}, n_m) = \frac{1}{\mathcal{Z}} \Omega(n_s, n_{str}, n_m) e^{-\beta E(n_s, n_{str}, n_m)} \tag{2.3}$$

where $\mathcal{Z}$ is the partition function, $\Omega(n_s, n_{str}, n_m)$ is the density of states and $\beta = 1/k_B T$ is the inverse temperature. Denoting with $\Omega_u(n_m)$ the density of unbound conformations, i.e. those with no contacts to the attractive wall,

and with $\Omega_b(n_\mathrm{s}, n_\mathrm{str}, n_\mathrm{m})$ the bound ones, i.e. with at least one contact to that wall, one can write the expression for the density of states as:

$$\Omega(n_\mathrm{s}, n_\mathrm{str}, n_\mathrm{m}) = \delta_{n_\mathrm{w},0}\Omega_u(n_\mathrm{m}) + (1 - \delta_{n_\mathrm{w},0})\Omega_b(n_\mathrm{s}, n_\mathrm{str}, n_\mathrm{m}), \tag{2.4}$$

where $n_\mathrm{w} = n_\mathrm{s} + n_\mathrm{str}$ is the total number of contacts to the attractive wall. If z_w denotes the distance between the steric and the attractive wall, as $z_\mathrm{w} \to \infty$, $\Omega_u(n_\mathrm{m}) \to \infty$ as well. Therefore, I will limit my work to values of z_w of the order of the chain length N. This leaves enough volume between both walls to allow some information from the free space to be detected. I choose $z_\mathrm{w} > N$ to allow for a completely expanded chain along the z axis with no wall contacts to exist which makes the effects of the steric wall insignificant to the study of adsorption.

2.3 The stripes

The attractive wall is patterned with parallel, equally spaced, stripes with equal width as illustrated in Figure 2.2. The distance between the left-most edges of neighbouring stripes is d, the width of each stripe is w. This gives a periodicity of length d on the x axis and the system does not change on the y axis. The interactions of the SAW with the stripes are modelled via the parameter $a = \epsilon_\mathrm{str}/epss$. Three distinct cases can be considered:

- $a < 0$, repulsion
- $a = 0$, no interaction
- $a > 0$, attraction.

The first case $a < 0$ is not being discussed in this work. The second one, $a = 0$, is equivalent to the case $a \gg 0$ with interchanging the roles of the stripes and the wall. The interval $a > 0$ can, furthermore, be divided in three:

- $0 < a < 1$, the stripes are less attractive than the wall
- $a = 1$, the surface is homogeneous
- $a > 1$, the stripes are more attractive than the wall.

The system with homogeneous attractive wall ($a = 1$) has already been studied in [13]. The case $0 < a < 1$ is equivalent to the case $a > 1$ with interchanging the roles of the stripes and the wall, therefore, only the case $a > 1$ is of interest for the present work.

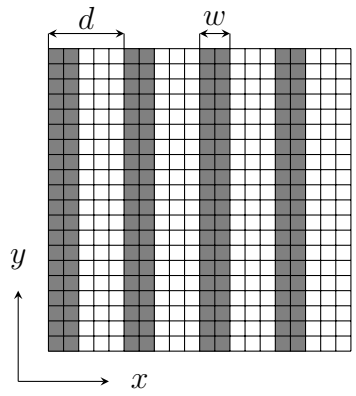

Figure 2.2: An example of a stripe-patterned wall. The stripes are indicated with a grey colour. The distance between the left-most edges of neighbouring stripes is $d = 5$. The width of each stripe is $w = 2$. The axes of the coordinate system are labelled with x and y.

2.4 Observables

The properties of the system are studied with the help of several observables, their temperature derivatives, variances and mutual covariances. The partition sum of the system is

$$\mathcal{Z} = \sum_{\sigma} e^{-\beta E(\sigma)} \tag{2.5}$$

and the expectation value of an observable $\mathcal{O}$ is

$$\langle \mathcal{O} \rangle = \frac{1}{\mathcal{Z}} \sum_{\sigma} \mathcal{O}(\sigma) e^{-\beta E(\sigma)}, \tag{2.6}$$

where the sums are performed over all possible states σ of the system. Extrema in the first temperature derivative of the expectation values deliver information about abrupt changes in the corresponding property, which yields information about existing phases. Analysing these functions per hand can be inconvenient, when the number of observables increases, therefore one needs a way of detecting these extrema with the help of a computer. There are two approaches that can be taken: use the data set to find all extrema with a sophisticated algorithm or use the second temperature derivative. The latter is trivial to implement and has been used here, since one only has to look for neighbouring points that are on the different sides of zero. There are also two approaches for calculating the temperature derivatives of expectation values of observables: by calculating the derivative numerically using

the data set and by calculating it via other observables. The latter has been utilised since it is straight forward and less error-prone for data from exact enumeration, which does not have statistical fluctuations like data from Monte Carlo (MC) simulations. The temperature derivatives are computed as follows:

$$\frac{\mathrm{d}\langle\mathcal{O}\rangle}{\mathrm{d}T} = \frac{1}{k_\mathrm{B}T^2}\left(\langle\mathcal{O}E\rangle - \langle\mathcal{O}\rangle\langle E\rangle\right) = \frac{1}{k_\mathrm{B}T^2}\mathrm{Cov}\left[\mathcal{O}, E\right] \tag{2.7}$$

$$\begin{aligned}\frac{\mathrm{d}^2\langle\mathcal{O}\rangle}{\mathrm{d}T^2} =& -\frac{2}{k_\mathrm{B}T^3}\left(\langle\mathcal{O}E\rangle - \langle\mathcal{O}\rangle\langle E\rangle\right) \\ &+ \left(\frac{1}{k_\mathrm{B}T^2}\right)^2\left(\langle\mathcal{O}E^2\rangle - 2\langle\mathcal{O}E\rangle\langle E\rangle + 2\langle\mathcal{O}\rangle\langle E\rangle^2 - \langle E^2\rangle\langle\mathcal{O}\rangle\right),\end{aligned} \tag{2.8}$$

where $\mathrm{Cov}\left[x, y\right] = \langle xy\rangle - \langle x\rangle\langle y\rangle$. Obviously this approach does not add that much complexity to the computer program since one needs to measure additionally only higher powers of E and multiplication of those with $\mathcal{O}$. All the extrema of all observables give a rough map of the phase diagram. The next step is to study the properties of each phase via the information that the observables themselves deliver.

The energy E gives the probability of finding the conformation at a specific temperature T. The total number of surface contacts $n_\mathrm{w} = n_\mathrm{s} + n_\mathrm{str}$ gives the fraction of the chain that is adsorbed onto the surface. This is also the part that is flat, i.e. two-dimensional. The number of stripe (surface, excluding stripes) contacts n_str (n_s) indicates what fraction of the chain lies on the stripes (surface, excluding stripes). The number of monomer-monomer contacts n_m describes the compactness of the chain, i.e. the more compact the chain, the larger n_m is.

The squared end-to-end distance R^2_ee indicates how extended the chain is:

$$R_\mathrm{ee} = \vec{r}_N - \vec{r}_1, \tag{2.9}$$

where $\vec{r}_i$ is the coordinate of the i-th monomer. The radius of gyration R^2_gyr describes the dimensions of the chain and its components R^2_{11}, R^2_{22} and R^2_{33} give the extensions of the SAW from its centre of mass on each axis:

$$R^2_\mathrm{gyr} = R^2_{11} + R^2_{22} + R^2_{33}, \tag{2.10}$$

with

$$R^2_{ij} = \frac{1}{N}\sum_{n=1}^{N}\left(r_i^{(n)} - \overline{r}_i\right)\left(r_j^{(n)} - \overline{r}_j\right), \tag{2.11}$$

where $r_i^{(n)}$ $(i = 1, 2, 3)$ is the i-th Cartesian coordinate of the n-th monomer and $\overline{r}_i = \sum_{n=1}^{N} r_i^{(n)}/N$. For clarity R_{11}^2, R_{22}^2 and R_{33}^2 will be denoted as $R_{\mathrm{gyr,x}}^2, R_{\mathrm{gyr,y}}^2$ and $R_{\mathrm{gyr,z}}^2$.

Rapid changes of the values of these quantities indicate phase boundaries and manifest themselves as extreme values in the temperature derivatives of the corresponding quantities. One of the most important is the heat capacity C_V that indicates the cumulative behaviour of all observables that are part of the energy E:

$$\begin{aligned} C_V =& \frac{\mathrm{d}\langle E\rangle}{\mathrm{d}T} = \frac{1}{k_{\mathrm{B}}T^2}\left(\langle E^2\rangle - \langle E\rangle^2\right) \\ =& \frac{\epsilon_s^2}{k_{\mathrm{B}}T^2}\left(\mathrm{Var}\left[n_{\mathrm{s}}\right] + b^2\mathrm{Var}\left[n_{\mathrm{m}}\right] + a^2\mathrm{Var}\left[n_{\mathrm{str}}\right]\right. \\ & \left. + 2b\mathrm{Cov}\left[n_{\mathrm{s}}, n_{\mathrm{m}}\right] + 2a\mathrm{Cov}\left[n_{\mathrm{s}}, n_{\mathrm{str}}\right] + 2ab\mathrm{Cov}\left[n_{\mathrm{m}}, n_{\mathrm{str}}\right]\right) \end{aligned} \tag{2.12}$$

where $\mathrm{Var}\left[x\right] = \mathrm{Cov}\left[x, x\right]$.

2.5 Studies of similar models

There are several analytic and Monte Carlo studies of the adsorption of ISAW onto a homogeneous surface in three dimensional lattice systems [13, 15, 16, 17]. They have found the existence of 4 main phases: desorbed-expanded (DE), desorbed-compact (DC), adsorbed-expanded (AE) and adsorbed-compact (AC). These works identified the boundaries between those phases, their shapes and the corresponding transitions in order to study the phase diagram of the systems. There exist also similar studies for off-lattice polymer models [18, 19].

Replacing the homogeneous surface with a patterned one introduces yet another main phase transition which is called recognition in this work. The shape of the phase diagram of this new system is studied and compared to the results for an off-lattice MC study of a similar polymer model by Monika Möddel [12] (see section 3.6).

2.6 Phases and transitions

Phase transitions in thermodynamics are defined for infinite systems. The difference to finite systems is that extreme points in the derivatives of the expectation values of canonical observables $\mathrm{d}\langle\mathcal{O}\rangle/\mathrm{d}T$ do not coincide. These

variations will furthermore be illustrated by the signals in different observables that give hints about pseudo-phase boundaries. The term phase would be used in what is to follow for clarity, but it should be noted that due to the finite sizes of the systems being investigated here, these are not phases but pseudo-phases.

2.6.1 Free chains

Starting with a free ISAW, the first observation that one makes when changing the temperature of the system is that at high temperatures the preferred conformations are extended with large energy and hence small number of monomer-monomer contacts, opposed to the low temperature regime where compact conformations with lots of self contacts are preferred (see Figure 2.3 for an illustration of the ground state of a chain with $N = 30$). One can identify two distinct transitions in finite systems. The first one is the coil-globule transition, where the polymer collapses from a coiled to a globular state with decreasing temperature as more self-contacts are favoured. This leads to a decrease of its spatial extension and thus a decrease in the radius of gyration. The transition temperature is the so-called Θ-point and the transition will be referred to as collapse. Another transition takes place below the Θ-point (at lower temperatures) when even the globule is compacted by further increasing the number of self-contacts. This will be referred to as freezing.

The energy of a free chain is $E = -\epsilon_{\mathrm{m}} n_{\mathrm{m}}$, which without loss of generality can be written as $E = -xy$. One can absorb the energy scale x in the temperature T by a simple transformation $(E, T) \leftrightarrow (E', T')$. Using $\beta' = 1/k_{\mathrm{B}}T'$ it is easy to show that $E\beta = E'\beta' \Rightarrow \langle\mathcal{O}\rangle(E, T) = \langle\mathcal{O}\rangle(E', T')$:

$$\langle\mathcal{O}\rangle(E,T) = \frac{\sum_\sigma \mathcal{O}(\sigma) e^{-\beta E(\sigma)}}{\sum_\sigma e^{-\beta E(\sigma)}} = \frac{\sum_\sigma \mathcal{O}(\sigma) e^{-\beta' E'(\sigma)}}{\sum_\sigma e^{-\beta' E'(\sigma)}} = \langle\mathcal{O}\rangle(E',T'). \quad (2.13)$$

Solving for $E' = \lambda E = -\lambda xy$ gives $T' = \lambda T$, thus $\langle\mathcal{O}\rangle(E, T) = \langle\mathcal{O}\rangle(\lambda E, \lambda T)$. This notation makes it easy to see that a peak at a temperature T in the system with energy E will be detected at a temperature λT in the system with energy λE. Thus, increasing the self-interaction energy by a factor λ results in a linear shift of all transitions from temperatures T to higher temperatures λT. The monomer-monomer interaction energy is usually used to model a solvent, i.e. the larger its value, the worse the solvent and vice versa. The better the solvent, the better it screens the intermolecular attraction resulting in a lower value of ϵ_{m}. Thus, depending on the solvent quality and the temperature one expects to find a polymer in one of the mentioned phases.

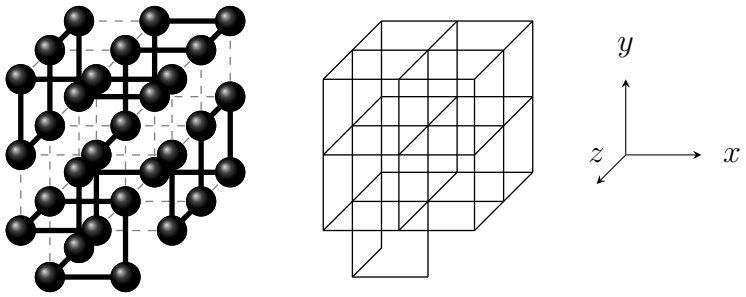

Figure 2.3: An example of a ground state of a free ISAW of $N = 30$ on the left. The solid line represents the ISAW, the monomers are indicated by circles and the monomer-monomer bonds by dashed lines. The ground state is a $3 \times 3 \times 3$ cube with 3 extra points on the bottom face. The cubical structure is illustrated on the right.

2.6.2 Attractive wall constraint

Introducing an attractive surface to the system results in two competing forces: monomer-surface attraction vs. monomer-monomer attraction. This changes the behaviour of the chains in the vicinity of the surface, where both forces compete. This leads to the distinction of two additional phases: adsorbed - a large fraction of the chain is on the surface and the opposite when a large fraction of the chain is free, i.e. desorbed. The collapse of the chains in the desorbed phase (away from the adsorption boundary) should be easy to detect, provided the collapse happens at a higher temperature than the adsorption. Near the adsorption transition, the collapse gets modified, since the monomer-monomer interactions compete with the monomer-surface interactions. How the modification takes place depends on the energy scales. The latter also influences the existence and form of the collapse transition in the adsorbed phase.

In the case of equal self- and wall-attraction ($b = 1$) the ground state of the ISAW is mostly two-dimensional for short chains. This is due to the small number of self-contacts that the chain can create. For a homogeneous surface a short chain should maximise self-contacts in two dimensions as illustrated in Figure 2.4. Longer chains have $n_{\mathrm{m}} > N$ which favours self-contacts to wall-contacts, thus creating a three-dimensional structure with one face attached to the wall. The latter is called a Surface Attached Globule (SAG). For $b > 1$ both the two and the three dimensional structures compete and which ones become ground states depends on the strength of the self attraction b and the chain length N.

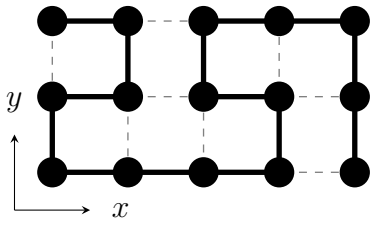

Figure 2.4: An example of a 2-dimensional ISAW of $N = 15$ and minimal energy. All points of a 3×5 rectangle have to be connected by the ISAW (solid line) in order to maximise the number of monomer-monomer contacts $n_{\mathrm{m}} = 8$ (dashed lines).

2.6.3 Attractive stripes

Introducing stripes to the attractive wall ($a > 1$) adds yet another competing force: the monomer-stripe attraction. For a large enough interaction, one would expect that large parts of the chain lay on one or several stripes, depending on the distance d between the stripes and the chain length N. For a larger interaction, the expectation would be that most of the chain lays on exactly one stripe, which would be called a recognised phase and the transition to it the recognition transition. The recognised phase is a sub phase of the adsorbed phase, since the stripes are part of the wall. Therefore, one would expect to find either a boundary between the recognised and the rest of the adsorbed phases, or a boundary between the recognised and the desorbed phases in case the recognised phase is the only constituent of the adsorbed phase.

One can discuss the ground states in the case $a \gg b$ since they are trivial. For narrow stripes ($w = 1$) the ground state conformation is one dimensional and non-degenerate. Wider stripes ($w = 2, 3, \ldots$) allow the chain to build self-contacts and thus allows lower energies for the ground state. The ground state conformations in that case are two-dimensional SAWs constrained to the stripe with maximum number of self-contacts n_{m} and are highly degenerate. In the other case when $a \gg b$ is not satisfied, the ground state conformations can be three-dimensional. That depends on the strength of the interactions a and b, the width of the stripe w as well as the length of the chain N and is not trivial.

Chapter 3

Exact Enumeration

3.1 Introduction

The first method that one can use in order to study a system is to generate all possible states of that system and calculate observables for each state. This method is called exact enumeration and gives one the possibility to compute the expectation values of all observables of interest over the chosen statistical ensemble. The data obtained in this way is exact and can also be used to verify the results of MC simulations. This gives a certain amount of confidence that the used algorithms work as expected and that no errors have been made in the process of writing the computer program.

The disadvantage of the method of exact enumeration is that it allows one to study only relatively small systems due to the enormous computational effort of generating all possible system states. The number of free SAW of length N in three dimensions is believed to be $c_N \propto \mu^N$, where μ is on the order of 5 [20], and thus gets large very fast as illustrated by the data in Table 3.1. Moreover, the computational time needed for generating all possible chains of a certain length grows faster than the number of chains possible, since the amount of computer memory that needs to be accessed grows too.

Using the resources provided by the Institute of Theoretical Physics of the University of Leipzig chains up to a length of $N = 19$ could be enumerated in reasonable time. A growth-based enumeration algorithm has been used to generate all possible SAW of length N from a fixed starting point (x_0, y_0, z_0). This allows for a trivial parallellization, where each possible starting point of the chain within the volume of the system could be enumerated independently. Each enumeration provides a density of states $\Omega(x_0, y_0, z_0, n_\mathrm{s}, n_\mathrm{str}, n_\mathrm{m})$. Combining the separate Ω for a chosen set of start-

Table 3.1: The number c_N of free SAW of length N in three-dimensions taken from the data in [20].

N	c_N	N	c_N	N	c_N
1	1	9	387 966	17	100 121 875 974
2	6	10	1 853 886	18	473 730 252 102
3	30	11	8 809 878	19	2 237 723 684 094
4	150	12	41 934 150	20	10 576 033 219 614
5	726	13	198 842 742	21	49 917 327 838 734
6	3 534	14	943 974 510	22	235 710 090 502 158
7	16 926	15	4 468 911 678	23	1 111 781 983 442 406
8	81 390	16	21 175 146 054	24	5 245 988 215 191 414

ing point coordinates $(x_1, y_1, z_1), \ldots, (x_n, y_n, z_n)$ gives the density of states for a complete system. Using the fact that the system does not change in the y direction, one value for the y coordinate of the starting point is sufficient. The starting points for a system with a cavity and parameters (z_w, d, w) are $\{(x, y, z) \mid 1 \leq x \leq d,\ y = 1,\ 1 \leq z \leq z_\mathrm{w}\}$.

A growth-based approach has been used for generating all possible chains X of length N originating from the point (x_0, y_0, z_0). Algorithm 1 using depth-first recursion has been utilised for that purpose. Starting with an empty chain X one invokes the recursion by calling the function GROW$((x_0, y_0, z_0), 1)$. Moreover, it is straightforward to turn this algorithm into a fast computer program.

Algorithm 1 GROW(x, n).

Ensure: x is a free point
  append x to the chain X
  if $n = N$ **then**
    compute *neighbours(x)*
    compute *observables*
  else
    compute *free-neighbours(x)*
    for i **in** *free-neighbours(x)* **do**
      call GROW$(i, n + 1)$
    end for
  end if
  remove x from the chain X

3.2 Calculation of observables

A more convenient way to handle equations (2.5) and (2.6) is to rewrite them as sums over the different types of contacts:

$$\mathcal{Z} = \sum_{n_\mathrm{m},n_\mathrm{s},n_\mathrm{str}} \Omega(n_\mathrm{m}, n_\mathrm{s}, n_\mathrm{str}) e^{-\beta E(n_\mathrm{m},n_\mathrm{s},n_\mathrm{str})} \tag{3.1}$$

$$\langle \mathcal{O} \rangle = \frac{1}{\mathcal{Z}} \sum_{n_\mathrm{m},n_\mathrm{s},n_\mathrm{str}} \mathcal{O}(n_\mathrm{m}, n_\mathrm{s}, n_\mathrm{str}) e^{-\beta E(n_\mathrm{m},n_\mathrm{s},n_\mathrm{str})} \tag{3.2}$$

with $\mathcal{O}(n_\mathrm{m}, n_\mathrm{s}, n_\mathrm{str})$ being the sum of $\mathcal{O}$ for conformations with the specified number of contacts:

$$\mathcal{O}(n_\mathrm{m}, n_\mathrm{s}, n_\mathrm{str}) = \sum_{\sigma} \mathcal{O}(\sigma)\, \delta_{n'_\mathrm{m},n_\mathrm{m}}\, \delta_{n'_\mathrm{s},n_\mathrm{s}}\, \delta_{n'_\mathrm{str},n_\mathrm{str}}\,. \tag{3.3}$$

In this way one only needs to store $\mathcal{O}(n_\mathrm{m}, n_\mathrm{s}, n_\mathrm{str})$ for every observable of interest from the exact enumeration and can introduce the parameters a, b and T later. This approach offers the possibility to explore the state space with just a single exact enumeration without the need to re-enumerate for every set of parameters.

3.3 Free chains

Exact enumeration has been done for free chains with $b = 1$ in order to identify the types and locations of phase transitions that can be detected. The ground state for $N = 15$ has $n_\mathrm{m} = 11$, while the ground state for $N = 18$ has $n_\mathrm{m} = 16$. One can identify one distinct peak in each of the curves $\mathrm{d}\langle n_\mathrm{m}\rangle/\mathrm{d}T$, $\mathrm{d}\langle R^2_\mathrm{gyr}\rangle/\mathrm{d}T$ and $\mathrm{d}\langle E\rangle/\mathrm{d}T$ (see Figures 3.1 and 3.2):

- for $N = 15$ the peaks are located at $T = 0.6432(1)$ in $\mathrm{d}\langle n_\mathrm{m}\rangle/\mathrm{d}T$ and C_V, $T = 0.9028(1)$ in $\mathrm{d}\langle R^2_\mathrm{gyr}\rangle/\mathrm{d}T$
- for $N = 18$ the peaks are located at $T = 0.4858(1)$ in $\mathrm{d}\langle n_\mathrm{m}\rangle/\mathrm{d}T$ and C_V, $T = 1.0330(1)$ in $\mathrm{d}\langle R^2_\mathrm{gyr}\rangle/\mathrm{d}T$.

The peak in $\mathrm{d}\langle n_\mathrm{m}\rangle/\mathrm{d}T$ moves to lower temperature with increasing chain length, contrary to the peak in $\mathrm{d}\langle R^2_\mathrm{gyr}\rangle/\mathrm{d}T$ which moves to higher temperature.

The positions of the peaks in C_V indicating the collapse and the freezing transitions have been studied systematically for different chain lengths on the simple cubic lattice in [21]. It has been found that both transitions can

be detected as separate peaks in C_V for chains with a length of $N > 40$. Moreover, it has also been found that for these chains the position of the peak corresponding to the collapse transition moves to higher temperatures with increasing chain lengths. The position of the peak corresponding to the freezing transition, however, has been found to have a discontinuous behaviour. The temperature at which the peak is to be found decreases with increasing chain length up to a value $N = N_1$, where the temperature would jump for $N = N_1 + 1$ to a higher value and continuously decrease again up to another value of the chain length $N = N_2$. The data in that study shows that the peak corresponding to the freezing transition shifts to lower temperatures continuously for $15 \leq N \leq 18$ and jumps up again at $N = 19$. From this I would conclude that the peak in $\mathrm{d}\langle n_\mathrm{m}\rangle/\mathrm{d}T$ gives hints to the freezing transition, since it shifts to lower temperatures and the peak in $\mathrm{d}\langle R^2_\mathrm{gyr}\rangle/\mathrm{d}T$ indicates the collapse transition, since it shifts to a higher temperature going from $N = 15$ to $N = 18$. That would also agree with the fact that only one peak is detectable in C_V for $N = 15$ as one can see in Figure 3.1. Taking a longer chain with $N = 18$ the ratio of the maximum number of self-contacts to the chain length increases from $11/15 \approx 0.73$ to $16/18 \approx 0.88$. The distance in temperature between both transitions increases and one finds hints about them in C_V and $\mathrm{d}\langle R^2_\mathrm{gyr}\rangle/\mathrm{d}T$. There seems to be two peaks where one is quite dominating as can be seen in Figure 3.2.

The information about the locations of both transitions is used to make a rough guess about the expected location of these transitions, provided they exist, in the system with an attractive surface. Moreover, one can play with the magnitude of the self-attraction in order to shift the location of the peaks in temperature and look at other effects that might arise from these changes.

3.4 Chain in a cavity ($N = 15$)

The properties of the ISAW in a cavity have been studied using the method of exact enumeration. The distance between the bounding walls has been fixed to $z_\mathrm{w} = 2N + 1$ in this section, except when otherwise mentioned. The ground state of the system is a chain connected to the surface of the attractive wall: either laying flat on it completely ($n_\mathrm{w}/N = 1$) for small values of b or touching it with parts of the chain for larger values of b. The two-dimensional structure is due to the short length of the chain not allowing for lots of self-contacts. One can clearly distinguish between two main phases: adsorbed and desorbed and the transition between both is clearly identifiable as a peak in C_V. In the following I will discuss systems with different stripe widths and

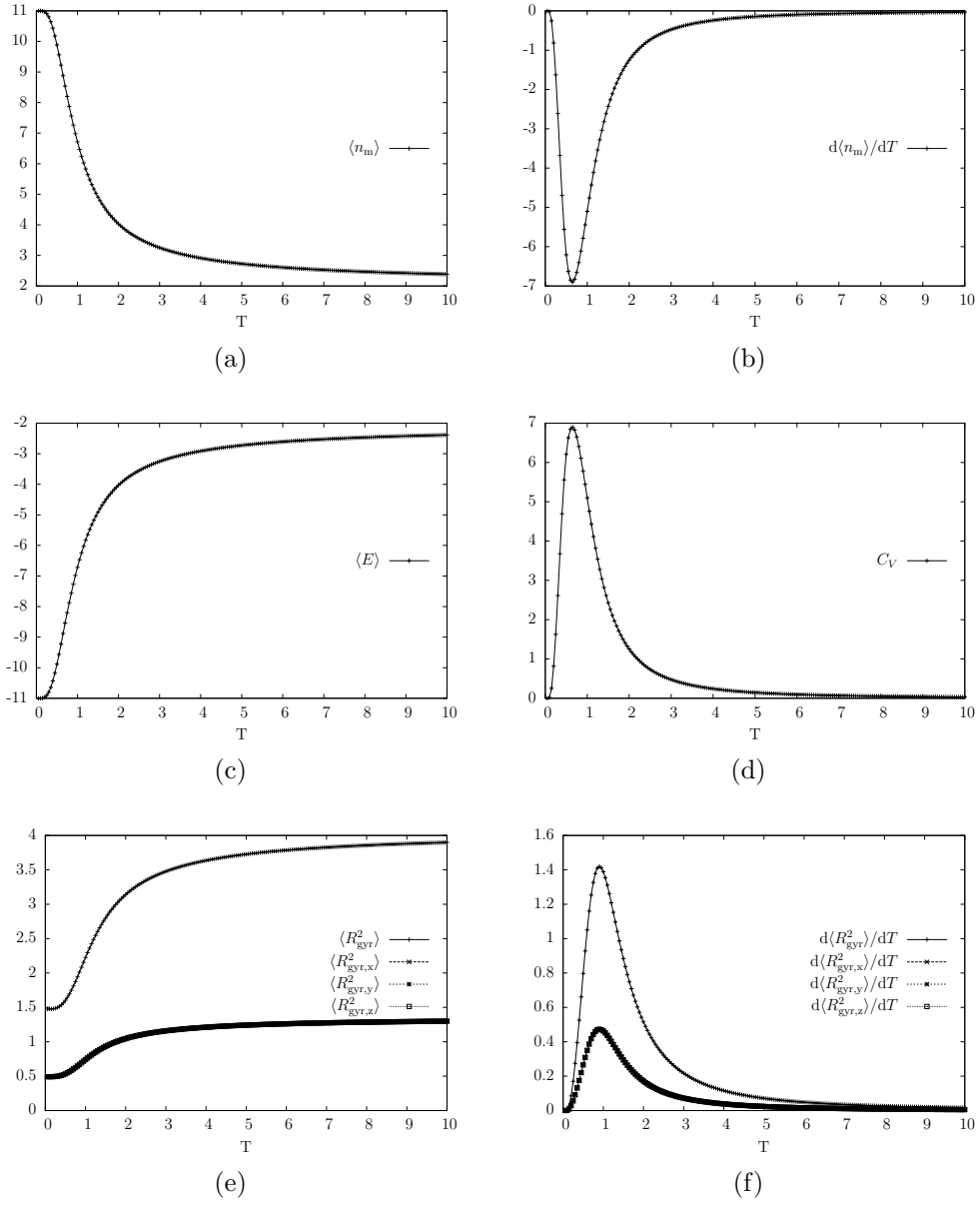

Figure 3.1: Canonical expectation values of important observables and their temperature derivatives for the parametrisation $N = 15$: (a) the number of self-contacts $\langle n_\mathrm{m}\rangle$; (c) the energy $\langle E\rangle$; (e) the squared radius of gyration $\langle R^2_\mathrm{gyr}\rangle$ and its components $\langle R^2_\mathrm{gyr,x}\rangle$, $\langle R^2_\mathrm{gyr,y}\rangle$ and $\langle R^2_\mathrm{gyr,z}\rangle$; (b), (d) and (f) show the temperature derivatives of (a), (c) and (e).

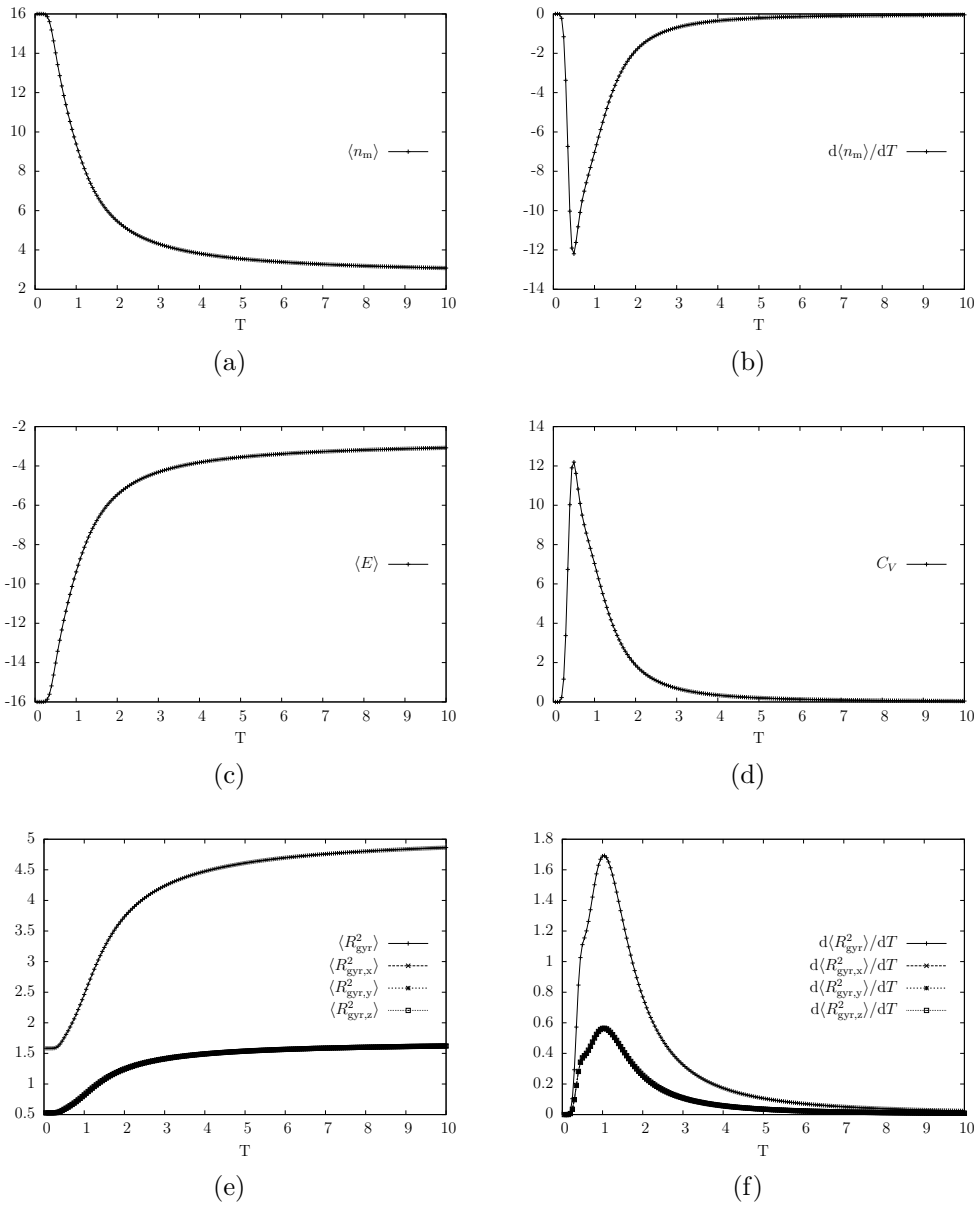

Figure 3.2: The same observables as in Figure 3.1, but for $N = 18$.

different monomer-monomer interaction strengths and their phase diagrams. The stripe distance has been fixed to $d = 5$. The chain length that is going to be discussed is fixed to $N = 15$.

3.4.1 Narrow stripes ($w = 1, b = 1$)

Three distinguished phases can be identified for this parametrisation: desorbed, adsorbed and recognised as can be seen in the phase diagram in Figure 3.3. Transitions can be clearly detected between the desorbed and adsorbed phases for all temperatures, between the adsorbed and the recognised phase for $T > 1.9$. There are some indications for a freezing transition in the low temperature ($T < 1$) adsorbed phase for $a < 1.9$, although the transition boundary is not that clearly identifiable. The boundary of the adsorption as well as the recognition transition is approximately linear in T for $a > 5$ and at first sight both are parallel. The slope of the adsorption transition can be extracted from a linear fit for $a > 5$ of each curve and is obtained as 0.63(1). The same procedure for the recognition transition yields 0.57(1) for the minima in $\mathrm{d}\langle R^2_{\mathrm{ee}}\rangle/\mathrm{d}T$ and 0.60(1) for the minima in $\mathrm{d}\langle R^2_{\mathrm{gyr}}\rangle/\mathrm{d}T$. Extrapolating for larger values of a one can speculate that both transitions would not merge, as the slope of the recognition transition is a bit smaller than the one of the adsorption transition. That, however, does not hold in general. It will be shown later on in section 3.4.3 that both can merge.

The desorbed phase is divided in two: "desorbed 1" and "desorbed 2". The boundary between both parts is barely detectable at first sight in $\mathrm{d}\langle R^2_{\mathrm{ee}}\rangle/\mathrm{d}T$ and $\mathrm{d}\langle R^2_{\mathrm{gyr}}\rangle/\mathrm{d}T$, since the maxima peaks are very small compared to the values of the curves for lower temperatures, so one has to zoom in to see the peaks. Though barely detectable, the boundary is there indicating the influence of the surface on the desorbed phase. That effect will be explained later on.

Adsorption

The adsorption transition can be identified as an approximately straight line in the phase diagram in Figure 3.3. It shifts to higher temperatures as the stripe attraction increases. To a first approximation, the shift is linear in a for $a > 5$. At low temperatures the whole chain is adsorbed, i.e. $\langle n_{\mathrm{w}}\rangle/N = 1$ and $\langle R^2_{\mathrm{gyr,z}}\rangle = 0$, as one can see in Figure 3.4. This means that the ground state is a two-dimensional SAW. The transition can be detected in the following observables:

- a negative minimum in $\mathrm{d}\langle n_{\mathrm{w}}\rangle/\mathrm{d}T$, i.e. as the temperature T increases

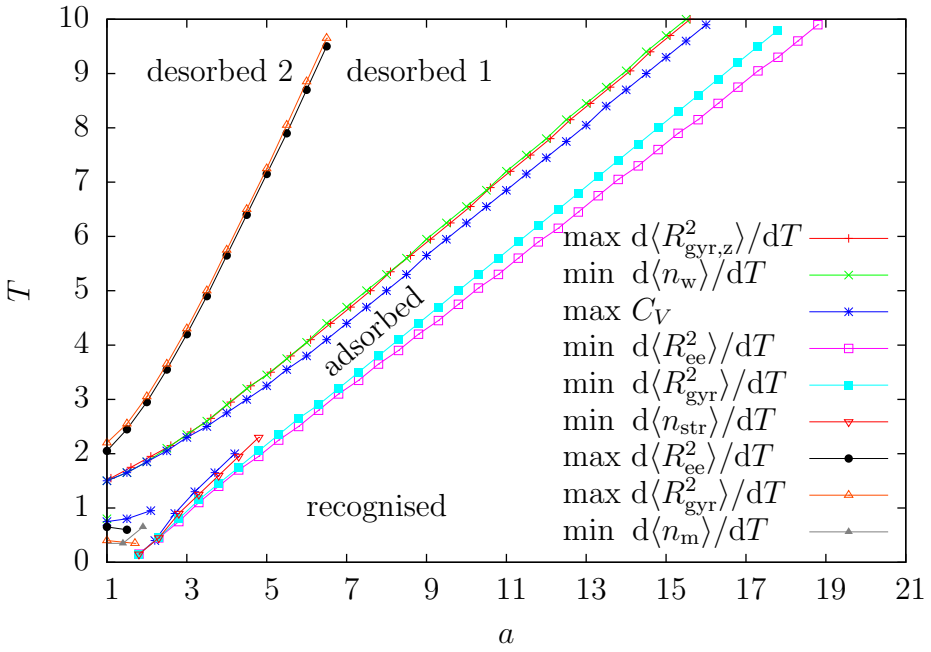

(a)

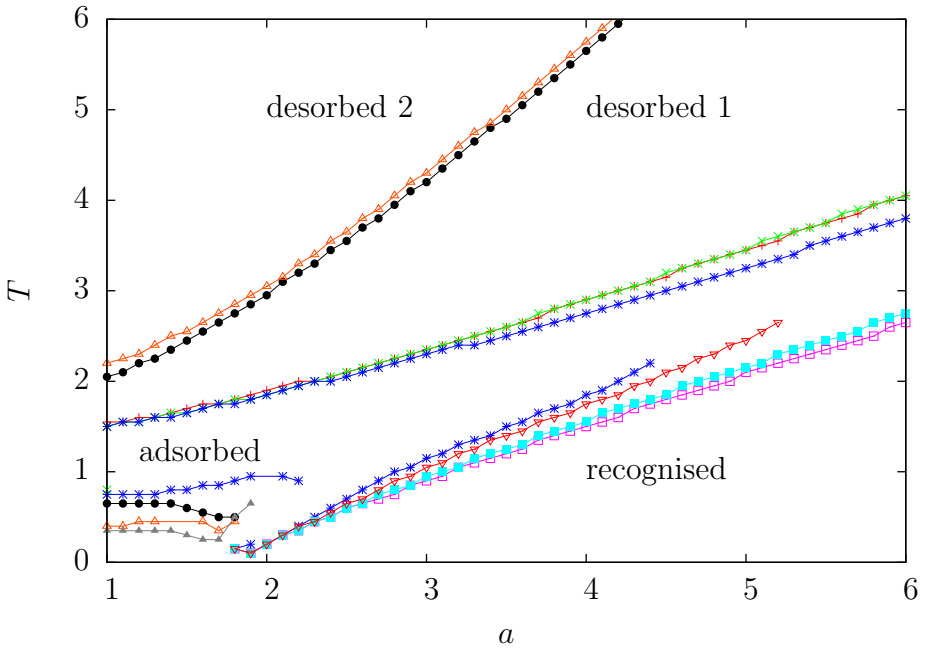

(b)

Figure 3.3: (a) the phase diagram of the system with (b) a zoom-in of the interesting part of the plot. The curves indicate minima or maxima of d⟨$\mathcal{O}$⟩/dT for different values of the monomer-stripe interaction a. The legend of (b) is the same as that of (a), every 5th data point is plotted in (a).

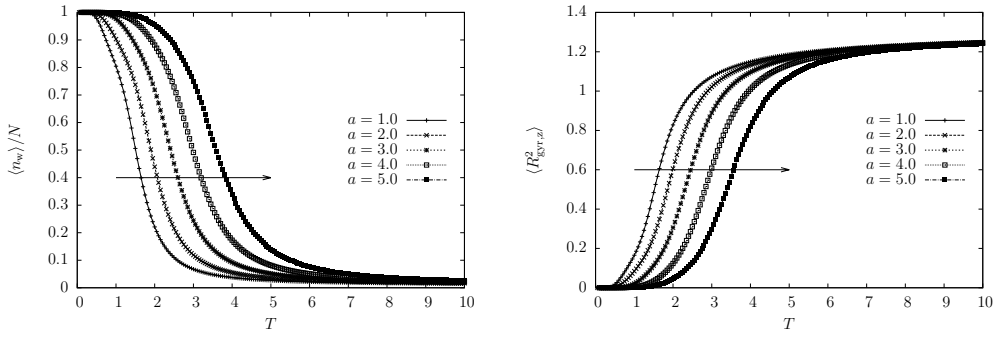

(a) (b)

Figure 3.4: (a) the expected number of wall contacts $\langle n_\mathrm{w} \rangle$ and (b) the expectation value of the z-component of the squared radius of gyration $\langle R^2_{\mathrm{gyr,z}} \rangle$ for different values of a. The arrow indicates increasing values of a.

the total number of contacts to the attractive wall decreases and the chain moves in the free space between both walls

- a positive maximum in $\mathrm{d}\langle R^2_{\mathrm{gyr,z}} \rangle / \mathrm{d}T$, i.e. as the temperature T increases larger parts are able to move freely in the z direction and are no longer connected to the wall

- a positive global maximum in C_V indicates the cumulative behaviour of the chain as the energy contributions from the wall decrease with increasing temperature T, it lays a bit off from the other two indicators because besides n_s and n_str another constituent is n_m which does not play any role in the adsorption; this maximum is also the highest one.

In this parametrisation I find a clear boundary separating the recognised phase from the rest of the adsorbed phase.

Freezing

The adsorption transition at this parametrisation can be located at values of $T > 1$. As identified in section 3.3, the expected freezing transition should be located near $T \approx 0.6$. Some indications about it can be found in the following observables:

- maximum in $\mathrm{d}\langle R^2_{\mathrm{gyr}} \rangle / \mathrm{d}T$ and $\mathrm{d}\langle R^2_{\mathrm{ee}} \rangle / \mathrm{d}T$, i.e. the chain expands with increasing temperature

- minimum in $\mathrm{d}\langle n_\mathrm{m}\rangle/\mathrm{d}T$, which indicates a transition from a compact two-dimensional chain to an extended one
- a maximum in C_V

The transition temperature of the freezing does not seem to be influenced by the value of the stripe attraction as long as one is not close to the recognition transition. Signals of the freezing transition are not detectable any more for $a > 1.9$, where the recognition starts to take place.

Recognition

The recognition transition is the transition where a chain adapts to the shape of a stripe. Depending on the value of a the ground state is a chain laying partly on a stripe or a chain laying completely on a stripe, i.e. the polymer recognises the stripe. One can see in Figure 3.6 that at low temperatures for $a \in [1.0; 1.6]$ approximately 1/3 of the chain is laying on a stripe and for $a \geq 2.0$ the full polymer is located on the stripe. Ground states corresponding to both parameter intervals are depicted in Figure 3.5. As expected for larger stripe attraction a the recognition transition shifts to higher temperatures. To a first approximation, the shift is linear for $a > 6$. The recognition transition can be detected in the following observables:

- a negative minimum in $\mathrm{d}\langle n_\mathrm{str}\rangle/\mathrm{d}T$ as the chain detaches from the stripe at higher temperatures
- negative minima in $\mathrm{d}\langle R^2_\mathrm{gyr}\rangle/\mathrm{d}T$ and $\mathrm{d}\langle R^2_\mathrm{ee}\rangle/\mathrm{d}T$ as the chain is not stretched along the stripe that much at higher temperatures
- a maximum in C_V

Collapse

There is no clear collapse transition detectable, although there are positive maxima in $\mathrm{d}\langle R^2_\mathrm{gyr}\rangle/\mathrm{d}T$ and $\mathrm{d}\langle R^2_\mathrm{ee}\rangle/\mathrm{d}T$ for $T > 2$. The boundary formed by the maxima separates what I call here the phases "desorbed 1" and "desorbed 2" in Figure 3.3. In the latter phase, the chain has almost no self-contacts as can be seen in Figure 3.7 ($\langle n_\mathrm{m}\rangle/N < 0.2$) and is a bit stretched. Going to lower temperatures the boundary to "desorbed 1" indicates that there the chain begins to create some self-contacts. The fraction of self-contacts created is quite low and hence the values of $\langle R^2_\mathrm{ee}\rangle$ and $\langle R^2_\mathrm{gyr}\rangle$ are large too. Therefore, the chain has not collapsed and this is not a collapse transition

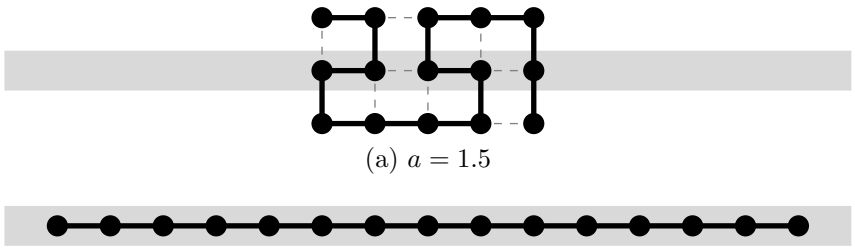

(a) $a = 1.5$

(b) $a = 3.5$

Figure 3.5: Ground states of the system with: $a = 1.5$ (a) and $a = 3.5$ (b). The chain is indicated by connected black dots representing the monomers. The thick grey line illustrates a stripe.

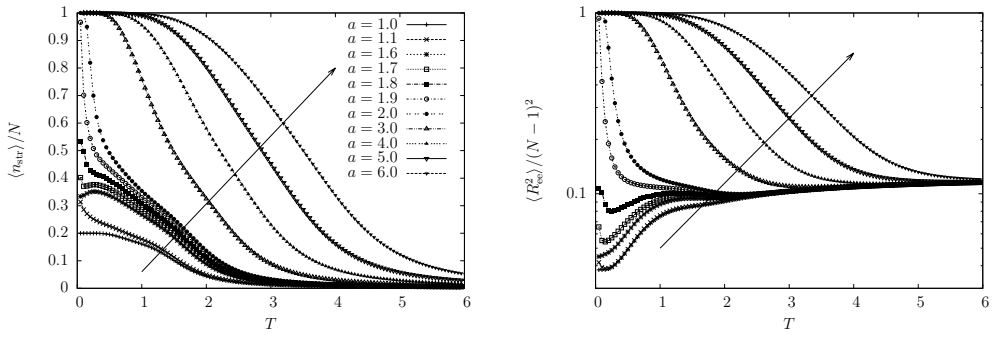

(a) (b)

Figure 3.6: (a) the expected number of stripe contacts $\langle n_{\rm str}\rangle$ and (b) the expectation value of the squared end-to-end distance $\langle R^2_{\rm ee}\rangle$ for different values of a. The arrow indicates increasing values of a. The legend of (b) is the same as that of (a).

in the sense of a free chain. It is merely an indicator of the free chain starting to feel the surface. This pure mathematical effect can be understood by looking at the behaviour of $\langle R^2_{\mathrm{ee}} \rangle$ and $\langle R^2_{\mathrm{gyr}} \rangle$. For a free chain their values decrease (Figure 3.1e) with decreasing temperature and at the point of greatest decrease one gets a peak in the derivative at T_{collapse}, which indicates the position of the collapse transition. For the system in question here, there is another effect at low temperature: the chain gets two-dimensional when adsorbed and even one-dimensional when completely attached to a stripe. This makes the values of both observables increase with decreasing temperature. This competition can be seen in Figure 3.6b: the larger the value of a the larger the value of T where the increase in $\langle R^2_{\mathrm{ee}} \rangle$ and $\langle R^2_{\mathrm{gyr}} \rangle$ sets on, thus deforming the part of the curve where the collapse would have been detected as the greatest increase. This deformation still allows one to detect a greatest increase for larger values of T, since the curve increases nevertheless. Hence, a greatest increase should be measurable somewhere in the part of the curve that has not been deformed much, leading to small peaks in $\mathrm{d}\langle R^2_{\mathrm{ee}} \rangle / \mathrm{d}T$ and $\mathrm{d}\langle R^2_{\mathrm{gyr}} \rangle / \mathrm{d}T$. Since in this parametrisation the collapse is not detectable in the desorbed phase, the line between "desorbed 1" and "desorbed 2" could have been skipped and the phase could have been labelled only as "desorbed", but that would have not been easy in the parametrisations that are to follow ($b = 5$), where the implications of this line become obvious. Moreover, the collapse transition, when located in the desorbed phase, should always take place at the same temperature. That would have led to a horizontal straight line in the phase diagram in Figure 3.3, which is obviously missing.

The system at $a = 1.5$

The ground state in this parametrisation is a two-dimensional chain laying on the attractive wall with 5 stripe- and 8 self-contacts. These values can be read from the data in Figure 3.8a. The conformation has the structure depicted in Figure 3.5a (laying on one stripe with the long side parallel to the stripe). Figure 3.8 shows the temperature dependence of the expectation values of some of the measured observables and their temperature derivatives. As the temperature increases the number of stripe-contacts increases resulting in a positive peak in $\mathrm{d}\langle n_{\mathrm{str}} \rangle / \mathrm{d}T$ at $T \approx 0.15$ thus breaking some self-contacts resulting in a negative peak in $\mathrm{d}\langle n_{\mathrm{m}} \rangle / \mathrm{d}T$ at $T \approx 0.25$. This decrease of self-contacts is also detectable as the first shoulder in C_V. Less self-contacts in this case mean that the chain elongates along the x-axis resulting in the positive peak in $\mathrm{d}\langle R^2_{\mathrm{gyr,x}} \rangle / \mathrm{d}T$ at $T \approx 0.3$ and the one negative in $\mathrm{d}\langle R^2_{\mathrm{gyr,y}} \rangle / \mathrm{d}T$ at $T \approx 0.25$. As the temperature increases further, parts of the chain start to detach from the surface. This results in negative values and a shoulder in

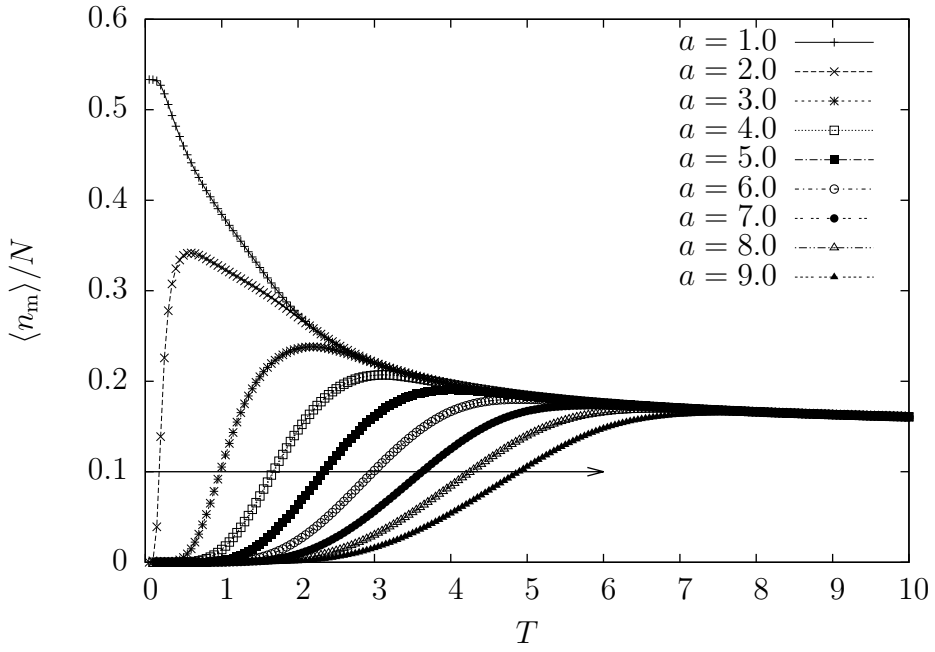

Figure 3.7: The expected number of self-contacts $\langle n_\mathrm{m} \rangle$ for different values of a. The arrow indicates increasing values of a.

$\mathrm{d}\langle n_\mathrm{w} \rangle / \mathrm{d}T$. The latter is detectable as the first peak in C_V at $T \approx 0.8$. Going to higher temperatures, large parts of the chain start to detach from the wall. This produces the second peak in C_V at $T \approx 1.65$, which comes from the decrease of wall contacts. The latter is detectable as a peak in $\mathrm{d}\langle n_\mathrm{w} \rangle / \mathrm{d}T$ at the same temperature. The detachment from the surface is also detectable as a positive maximum in $\mathrm{d}\langle R^2_{\mathrm{gyr,z}} \rangle / \mathrm{d}T$ at the same temperature, showing that the chain expands in the z-dimension.

The system at $a = 3.5$

The ground state in this parametrisation is a chain stretched along a stripe ($n_\mathrm{str}/N = 1$) and with no monomer-monomer contacts ($n_\mathrm{m} = 0$) as depicted in Figure 3.5b. Figure 3.9a shows the temperature dependence the expectation values of some of the measured observables and their temperature derivatives. As the temperature increases, a fraction of the chain detaches from the stripe but stays attached to the surface of the wall. This allows the formation of self-contacts resulting in the positive peaks in $\mathrm{d}\langle n_\mathrm{s} \rangle / \mathrm{d}T$ and $\mathrm{d}\langle n_\mathrm{m} \rangle / \mathrm{d}T$ at $T \approx 1.3$ and a negative one in $\mathrm{d}\langle n_\mathrm{str} \rangle / \mathrm{d}T$ at $T \approx 1.4$, plotted in Figure 3.9b. The decrease in stripe contacts gives, furthermore, rise to the

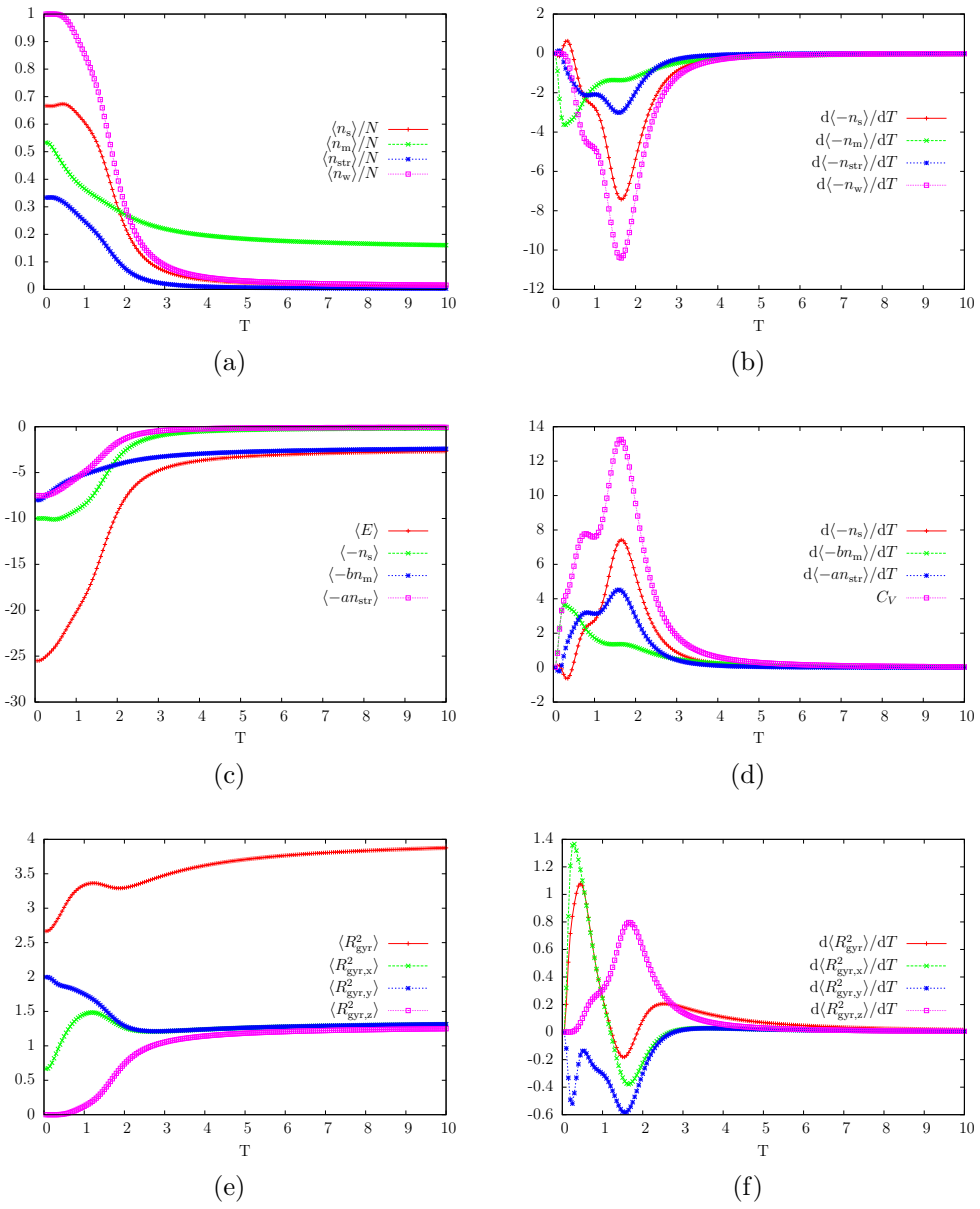

Figure 3.8: Canonical expectation values of important observables and their temperature derivatives for $a = 1.5$: (a) the number of self-contacts $\langle n_\mathrm{m}\rangle$, the number of surface contacts without stripes $\langle n_\mathrm{s}\rangle$, the number of stripe contacts $\langle n_\mathrm{str}\rangle$ and the number of total wall contacts $\langle n_\mathrm{w}\rangle$ normalised to the length of the chain; (c) the energy $\langle E\rangle$ and its components $\langle -n_\mathrm{s}\rangle$, $\langle -bn_\mathrm{m}\rangle$ and $\langle -an_\mathrm{str}\rangle$; (e) the squared radius of gyration $\langle R^2_\mathrm{gyr}\rangle$ and its components $\langle R^2_\mathrm{gyr,x}\rangle$, $\langle R^2_\mathrm{gyr,y}\rangle$ and $\langle R^2_\mathrm{gyr,z}\rangle$; (b), (d) and (f) show the temperature derivatives of (a), (c) and (e), respectively.

low temperature peak in C_V at $T \approx 1.5$ (Figure 3.9d) as the system enters the adsorbed phase. As the temperature increases further, the number of wall contacts decrease rapidly resulting in a negative peak in $\mathrm{d}\langle n_{\mathrm{w}}\rangle/\mathrm{d}T$ at $T \approx 2.6$, giving rise to the high temperature peak in C_V at $T \approx 2.5$ and the system undergoes a transition into the desorbed phase.

Information about the changes in the shape of the chain can be found in the negative peak in $\mathrm{d}\langle R^2_{\mathrm{gyr,y}}\rangle/\mathrm{d}T$ at $T \approx 1.3$ and the positive one in $\mathrm{d}\langle R^2_{\mathrm{gyr,x}}\rangle/\mathrm{d}T$ at $T \approx 1.5$, indicating that the chain undergoes a transition from the stretched shape along the stripe, i.e. along the x-axis, to shapes that extend also along the y axis. Another shape transition can be located at a higher temperature in $\mathrm{d}\langle R^2_{\mathrm{gyr,z}}\rangle/\mathrm{d}T$ at $T \approx 2.6$, indicating that the chain changes its shape from a flat (two-dimensional) to a three-dimensional conformation.

Estimating the position of the recognition transition at low temperatures

Knowing the ground states of the chain in the recognised and the rest of the adsorbed phase one can make a rough estimate of the position of the recognition transition. The energy of the recognised chain is $E_{\mathrm{recognised}} = E(0, 15, 0) = -15a$ (see Figure 3.5b), the energy of the chain at say $a = 1.5$ is $E_{\mathrm{adsorbed}} = E(10, 5, 8) = -18 - 5a$ (see Figure 3.5a). Solving $E_{\mathrm{adsorbed}} - E_{\mathrm{recognised}} = 0$ for a yields $a = 1.8$ meaning that:

- $E_{\mathrm{adsorbed}} < E_{\mathrm{recognised}}$, for $a \leq 1.8$
- $E_{\mathrm{adsorbed}} > E_{\mathrm{recognised}}$, for $a \geq 1.8$

which agrees approximately with the position of the recognition transition in the phase diagram in Figure 3.3b.

Microcanonical Analysis

Looking for first-order phase transitions, one can also perform a microcanonical analysis of the system using the computed density of states. Detailed information about the theory of microcanonical thermodynamics of finite systems can be found in [22]. This kind of analysis allows one to detect transitions with phase coexistence. For that purpose one needs to look at the density of states in Figure 3.10a. If one is able to find a tangent line to the entropy $S(E) = k_{\mathrm{B}} \log \Omega(E)$ that is a tangent at two points of the curve and does not intersect the curve at any other points, then the inverse slope of that line is the transition temperature. One can easily fit tangent lines to $S(E)$

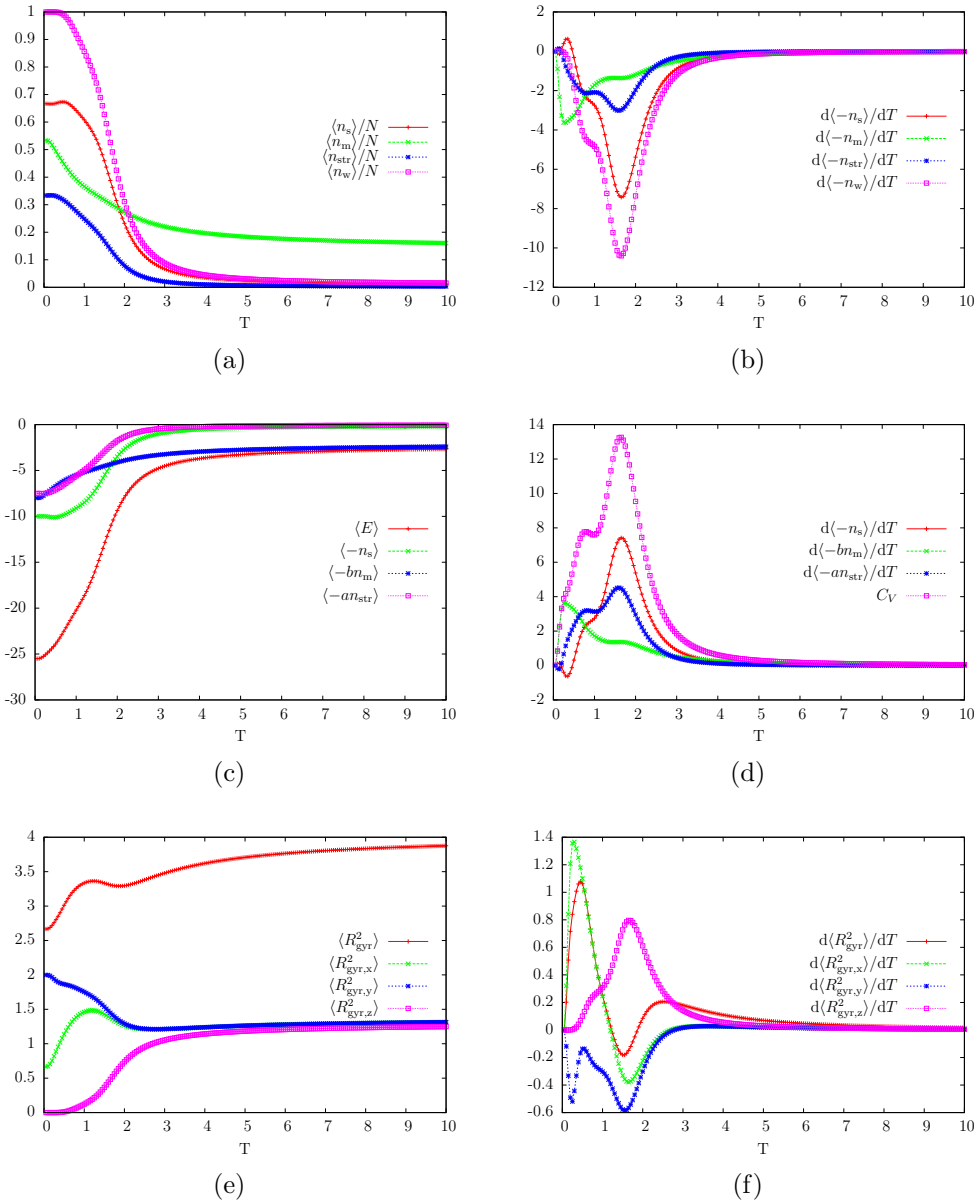

Figure 3.9: The same as Figure 3.8 but for $a = 3.5$.

per hand, but taking a parametrisation with non-integer values of a (as in Figure 3.10b) changes things completely. Due to the lattice, only states with discrete energy values exist, moreover due to the self-avoidance and the wall constraint only states with a certain combination of the number of contacts $(n_{\mathrm{s}}, n_{\mathrm{str}}, n_{\mathrm{m}})$ are allowed. This creates a quite messy picture of the density of states for some non-integer combinations of the parameters a and b. In order to extract the transition temperatures for each parametrisation I used the following automated approach:

1. compute $S(E)$
2. for each pair (E_i, E_j) solve the system of equations

$$\begin{cases} S(E_i) = a_{ij} + b_{ij}E_i \\ S(E_j) = a_{ij} + b_{ij}E_j \end{cases}$$

   for a_{ij} and b_{ij}, thus defining the linear function $f_{ij}(E) = a_{ij} + b_{ij}E$ that passes through the points $(E_i, S(E_i))$ and $(E_j, S(E_j))$
3. if $f_{ij}(E) \geq S(E)\ \forall E$ [1], then $T = 1/b_{ij}$ is the microcanonical transition temperature.

Using this method I could obtain the adsorption and the recognition transition curves plotted in Figure 3.11. There are a few horizontal lines in the plot that are located in the desorbed region. They correspond to the high energy peak region in $\Omega(E)$ (Figure 3.10a) and come from neighbouring energy values, on which tangent lines with a small slope can be fitted. These horizontal lines can easily be filtered out by requiring that the tangents are fitted through energy values E_i and E_j some distance apart. Requiring $|E_i - E_j| > b$ seems a good rule of thumb in this case, since the minimum energy change in the high energy phase is b. This yields the plot in Figure 3.11b, where one can clearly identify the adsorption and recognition transition lines. As one can see, the phase boundaries are well defined lines for large values of a, opposed to the curves on the canonical phase diagram. The slope of the recognition transition boundary is 0.6000(1) and the slope of the adsorption transition boundary for $a > 7$ is 0.5988(1).

[1] This step cannot be done as written on a computer, because $f_{ij}(E) \geq S(E)$ is not always fulfilled for $E \in \{E_i, E_j\}$ when using floating point numbers with finite precision in the numerical calculations of $f_{ij}(E)$. The latter criteria can be in practise rewritten as $f_{ij}(E) + \epsilon_{num} \geq S(E)$. I used $\epsilon_{num} \approx 1000 \times 10^{-16}$ for calculations with double precision floating point numbers (IEEE 754) with the hope that it would give me enough precision to detect the functions $f_{ij}(E)$ giving me first-order phase transitions without much false positives.

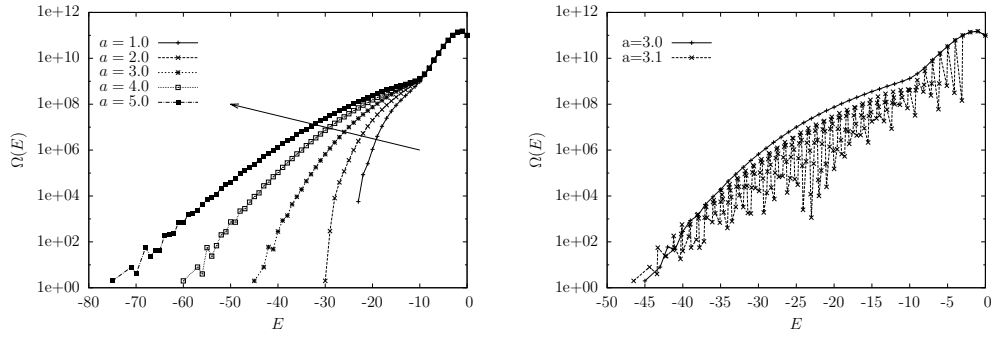

(a) (b)

Figure 3.10: The density of states of the system for: (a) integer values of a and (b) a non-integer value of a . The arrow indicates increasing value of a.

In order to better understand the transitions, let's first take a look at the construction of the tangents to $S(E)$. Figure 3.12 gives an example for $a = 5$. The line corresponding to the adsorption transition touches $S(E)$ at $E = -2$ and $E = -39$. The line corresponding to the recognition transition touches $S(E)$ at $E = -68$ and $E = -75$. The latter line is interesting, because (for large enough values of a, where one can detect the recognition transition) it connects the lowest energy state ($E_1 = E(0, N, 0)$, $\Omega(E_1) = 2$) with what seems to be a small peak in $S(E)$. The energy corresponding to that peak is $E_2 = E(2, N-2, 1)$. This is the set of all conformations laying onto a stripe with all but two monomers, which lay on the rest of the wall and allow the chain to form one self-contact. Such a conformation is depicted in Figure 3.13. The total number of such conformations is $\Omega(E_2) = 56$. Knowing this, one can calculate the microcanonical temperature corresponding to the transition between these two states:

$$T = \frac{E_2 - E_1}{\log(\Omega(E_2)) - \log(\Omega(E_1))} = \frac{E_2 - E_1}{\log(\Omega(E_2)/\Omega(E_1))}. \tag{3.4}$$

This yields $T = (2a - 2 - b)/\log(28) = (2a - 3)/\log(28)$. This expression for the temperature of the recognition transition gives the line in Figure 3.11. Moreover, it is an analytic expression that allows one to also estimate the value of a where the recognition transition would start to appear:

$$a = \lim_{T \to 0} \frac{T \log(28) + 2 + b}{2} = 1 + \frac{b}{2} = 1.5 \tag{3.5}$$

This value is close to the previous estimation of $a = 1.8$. Doing the same kind of analysis in order to obtain an analytic expression for the ad-

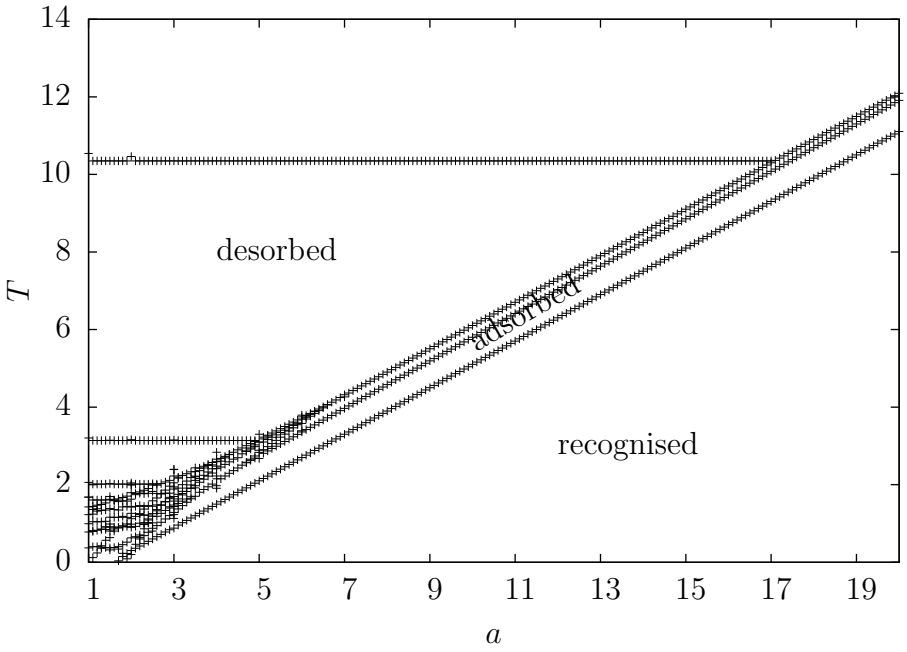

(a) $|E_i - E_j| > 0$

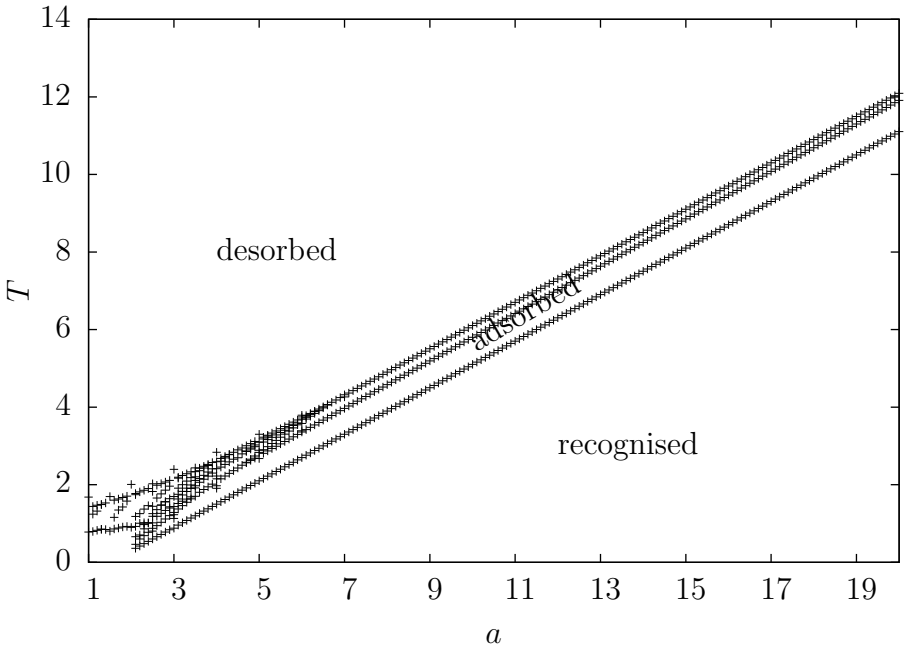

(b) $|E_i - E_j| > 1$

Figure 3.11: The phase diagram recovered from the microcanonical analysis for two different variations of the method described in 3.4.1: one allowing $|\min(E_i - E_j)| > 0$ (a) and the other allowing $|E_i - E_j| > 1$ (b). The points indicate transition temperatures computed from the density of states for different values of a in the parametrisation $b = 1$.

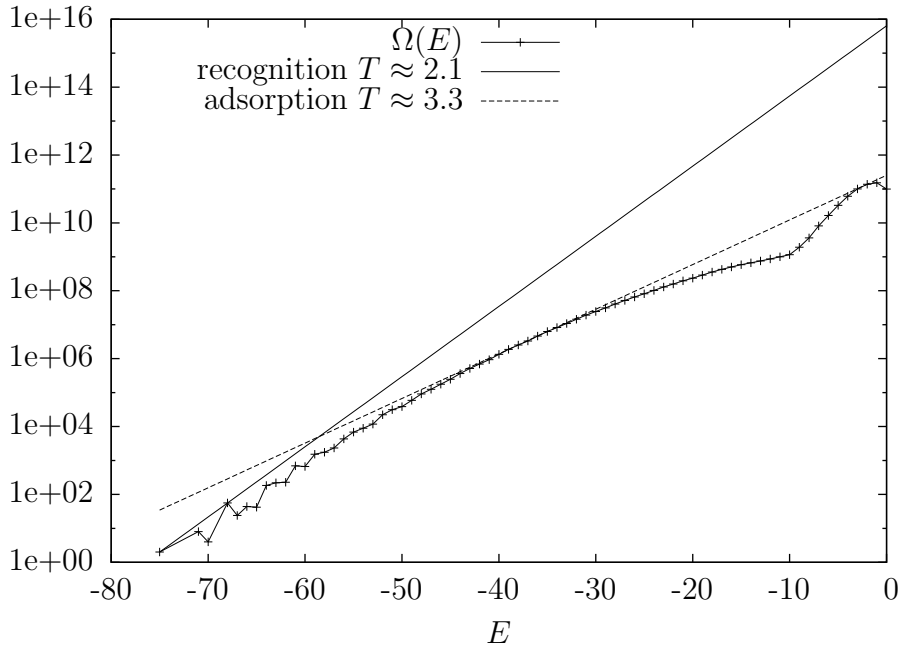

Figure 3.12: The construct for calculating the microcanonical transition temperature from the density of states $\Omega(E)$ for $a = 5$. The two lines are the tangents to the entropy $S(E)$ and correspond to the recognition and the adsorption transitions. The inverse slope of the lines is given as the temperature of each transition.

sorption transition would be quite difficult, due to the high entropy of the conformations involved.

3.4.2 Narrow stripes ($w = 1, b = 5$)

Increasing the strength of the self-attraction results in a linear shift of the collapse and the freezing transitions for a free chain. The self-attraction is chosen to be $b = 5$ in this section, thus shifting the collapse of the free chain to $T \approx 4.5$. This temperature is above the adsorption transition temperature for small values of a and allows the observation of collapse in the desorbed phase, thus changing the phase diagram. Moreover, it forces the appearance of other phases that would otherwise be observed at $b = 1$ in long chains. Longer chains allow for higher number of self-contacts per unit length (n_{m}/N) which allows for higher contributions to the value of the energy compared to the other interactions and allows the energy to fluctuate more. Taking a

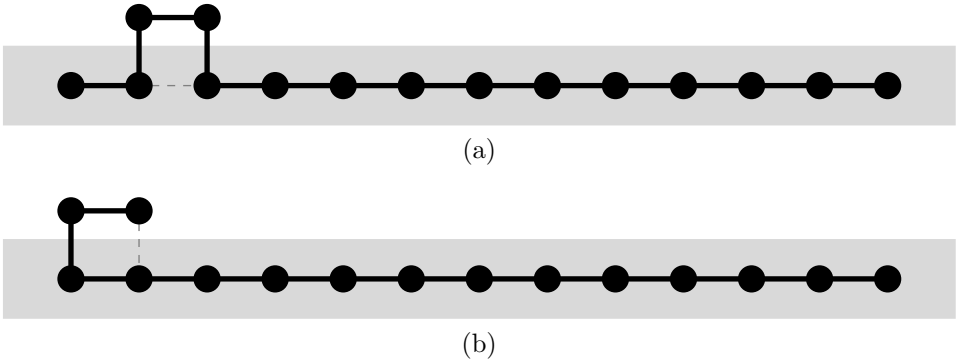

(a) (b)

Figure 3.13: Example conformations with energy $E(2, N-2, 1)$. The thick grey line illustrates a stripe.

look back at the definition of the energy of the chain:

$$E(n_{\mathrm{s}}, n_{\mathrm{str}}, n_{\mathrm{m}}) = -\epsilon_{\mathrm{s}} n_{\mathrm{s}} - \epsilon_{\mathrm{str}} n_{\mathrm{str}} - \epsilon_{\mathrm{m}} n_{\mathrm{m}} \tag{2.1}$$

normalising to the length of the chain:

$$E(n_{\mathrm{s}}, n_{\mathrm{str}}, n_{\mathrm{m}})/N = -\epsilon_{\mathrm{s}} \frac{n_{\mathrm{s}}}{N} - \epsilon_{\mathrm{str}} \frac{n_{\mathrm{str}}}{N} - \epsilon_{\mathrm{m}} \frac{n_{\mathrm{m}}}{N} \tag{3.6}$$

and having in mind that $\max(n_{\mathrm{s}}/N) = \max(n_{\mathrm{str}}/N) = 1$ where $\max(n_{\mathrm{m}}/N) = O(4)$ with $O(4) < 4$, one can easily see that for $N = 15$, $b \max(n_{\mathrm{m}}/N) \approx 3.7$ gives comparable energy contributions as longer chains. This artificial amplification of the self-interaction, that otherwise happens naturally in longer chains, gives the possibility to observe layering in the low temperature region. One can identify three different phases in the low temperature adsorbed region ($T < 1$):

- $a \in [1.1; 1.7]$, where $\langle n_{\mathrm{s}} \rangle = 6$, $\langle n_{\mathrm{str}} \rangle = 3$, $\langle n_{\mathrm{m}} \rangle = 11$
- $a \in [2.3; 4.9]$, where $\langle n_{\mathrm{s}} \rangle = 4$, $\langle n_{\mathrm{str}} \rangle = 4$, $\langle n_{\mathrm{m}} \rangle = 11$
- $a > 5.6$, where $\langle n_{\mathrm{s}} \rangle = 0$, $\langle n_{\mathrm{str}} \rangle = 15$, $\langle n_{\mathrm{m}} \rangle = 0$

The first two phases with $\langle n_{\mathrm{m}} \rangle = 11$ have compact chains formed in two layers, where one side of the structure is attached to a stripe and the rest of the surface. Example conformations from these phases are depicted in Figure 3.16 and Figure 3.17.

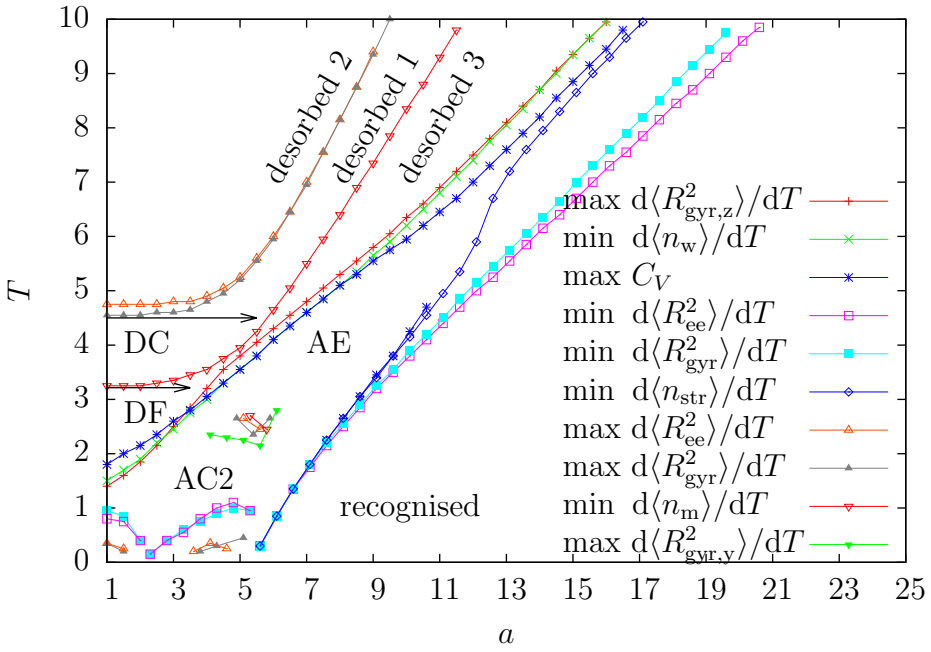

(a)

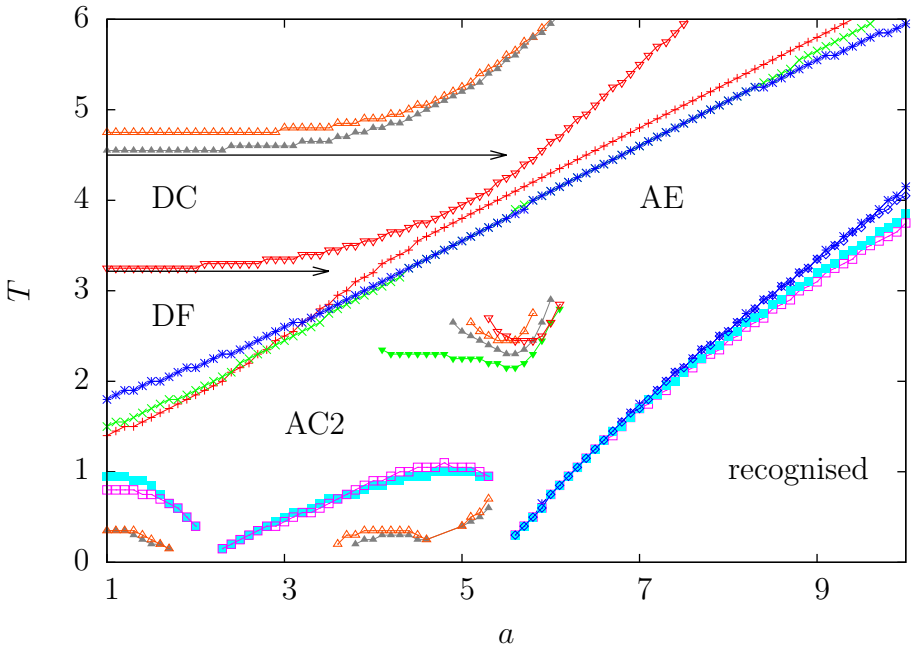

(b)

Figure 3.14: (a) the phase diagram of the system with (b) a zoom-in of the interesting part of the plot. The curves indicate minima or maxima of d⟨$\mathcal{O}$⟩/dT for different values of the monomer-stripe interaction a. The legend of (b) is the same as that of (a), every 5th data point is plotted in (a). The lines of the arrows indicate the position of the collapse and freezing transitions as calculated from the free chain. The heads of the arrows are used to outline the arrow lines from the rest of the curves and carry no physical information.

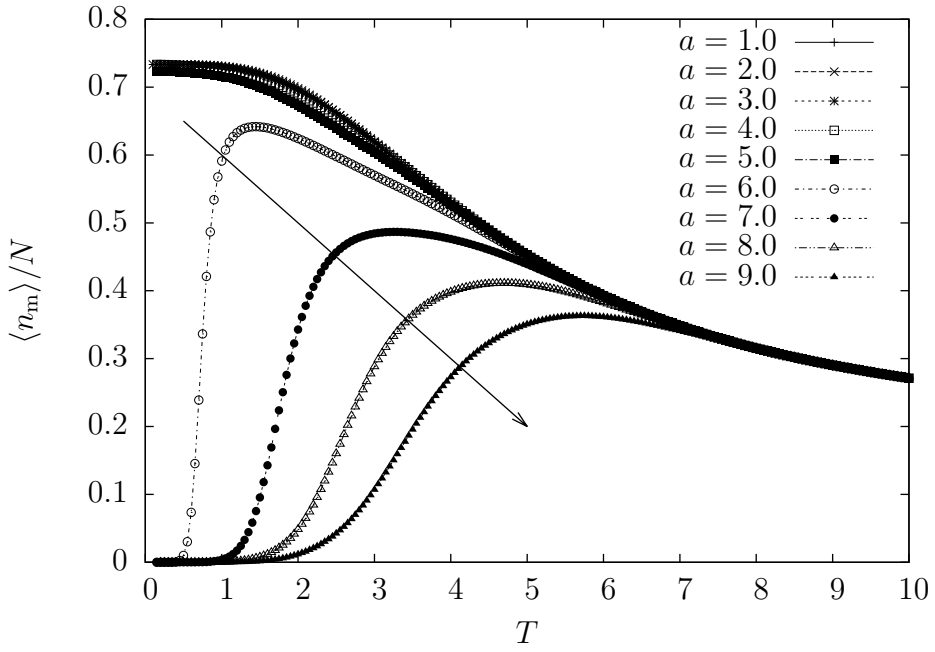

Figure 3.15: The expected number of self-contacts $\langle n_{\mathrm{m}} \rangle$ for different values of a. The arrow indicates increasing values of a.

Collapse

The collapse transition in this parametrisation can be identified with the horizontal straight line at about $T \approx 4.7$ for $a < 4$. For larger values of a the peaks in $\mathrm{d}\langle R^2_{\mathrm{ee}} \rangle / \mathrm{d}T$ and $\mathrm{d}\langle R^2_{\mathrm{gyr}} \rangle / \mathrm{d}T$ shift to higher temperatures due to the influence of the adsorption transition. The continuation of the horizontal line for $a > 4$ indicates only the positions of the peaks in the observables mentioned above. It does not indicate any collapse, since the number of self-contacts (plotted in Figure 3.15) at those temperatures is quite low, therefore indicating that the conformations are not globular. Both parts of the phase diagram separated by that line are named "desorbed 1" and "desorbed 2". The conformations in these regions have coil-like structure. The region below the collapse transition line is named "DC" - desorbed collapsed. This means that for those values of a, going to lower temperatures would allow the globular structures to be adsorbed onto the surface, which is known as the surface attached globule (SAG) phase.

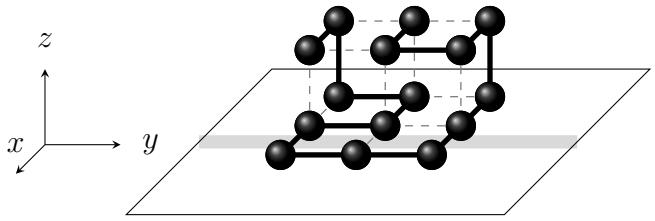

Figure 3.16: Conformation with $N = 15, n_{\mathrm{s}} = 6, n_{\mathrm{str}} = 3, n_{\mathrm{m}} = 11$. The thick grey line illustrates a stripe.

Freezing

A minimum in $\mathrm{d}\langle n_{\mathrm{m}}\rangle/\mathrm{d}T$ can be detected as a horizontal straight line in the phase diagram at about $T \approx 3.25$ for small values of a. Its position corresponds to the expected position of the freezing transition for a free chain with $b = 5.0$. That is at $T = 3.2160(5)$. The region between the freezing and the adsorption transition lines is labelled as the "DF" phase, i.e. desorbed-frozen. For larger values of a near the position of the adsorption transition, the line changes its slope and becomes an inclined straight line for $a > 5$. For those values at $a > 5$ the fraction of self-contacts is low (Figure 3.15). Therefore this cannot be called a freezing transition line in that region. The reason for the peak not staying at a constant temperature is the same effect as discussed for the behaviour of the collapse transition. This leads to a new phase between the "desorbed 1" and the "adsorbed" which is here labelled as "desorbed 3". The fact that this phase is detectable is consistent with the assumption that the adsorption transition should modify all transitions from the "desorbed" phase in the same way.

Adsorption

For small values of a the collapse transition takes place at a higher temperature than the adsorption transition. Therefore the adsorbed chains have globular form (SAG) with only a small number of wall contacts n_{w} as one can see in Figure 3.18. The ground state of the ISAW in the case of small a is composed of two layers as one can see from the value of $\langle R^2_{\mathrm{gyr,z}}\rangle \neq 0$. For values of $a < 1.7$ it has the ground state conformation of a free chain and is attached with one side to the wall as depicted in Figure 3.16. For values of $2.8 < a < 4.6$ elongated shapes along a stripe depicted in Figure 3.17 are preferable. For values of $a > 4.6$, no collapse can be clearly detected. For $a > 7$ the adsorption transition shifts to higher temperatures than the collapse transition and therefore no collapse is possible.

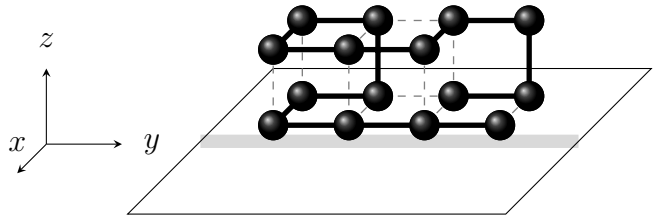

Figure 3.17: Conformation with $N = 15, n_{\mathrm{s}} = 4, n_{\mathrm{str}} = 4, n_{\mathrm{m}} = 11$. The thick grey line illustrates a stripe.

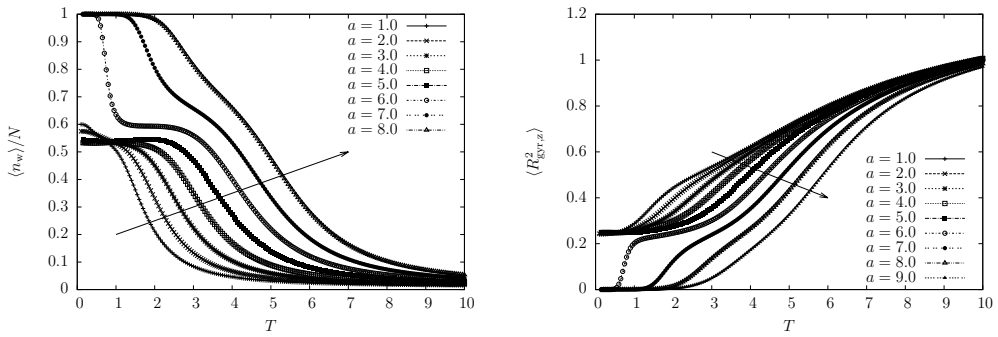

(a) (b)

Figure 3.18: (a) the expected number of wall contacts $\langle n_{\mathrm{w}} \rangle$ and (b) the expectation value of the z component of the squared radius of gyration $\langle R^2_{\mathrm{gyr,z}} \rangle$ for different values of a. The arrow indicates increasing values of a.

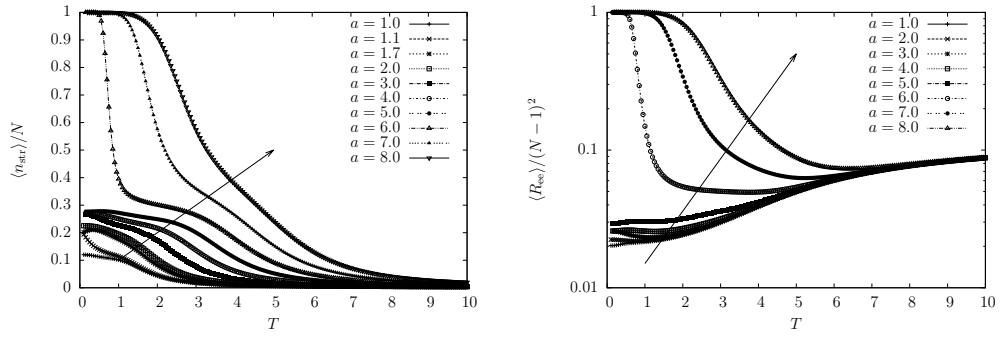

(a) (b)

Figure 3.19: (a) the expected number of stripe contacts $\langle n_{\rm str}\rangle$ and (b) the expectation value of the squared end-to-end distance $\langle R^2_{\rm ee}\rangle$ for different values of a. The arrow indicates increasing values of a.

Collapse of the adsorbed chain

The collapse transition can be detected in the adsorbed phase too. It is indicated by the small approximately horizontal lines at $T \approx 2.5$ for $4 < a < 6$. Above that line the conformations are two dimensional and that part of the phase is labelled here as "AE" (adsorbed extended). The larger a gets the more extended the chain becomes in "AE" as can be seen from the values of $\langle R^2_{\rm ee}\rangle$ in Figure 3.19b. The lower part of the adsorbed phase is labelled here as "AC2" to indicate that the chain is adsorbed, collapsed and forms two layers. Therefore, the transition line separating "AE" and "AC2" can be associated with the collapse transition. The chain having contacts with the attractive wall has less energy than the same chain with no contacts to the attractive wall. This results in a shift of the temperature of the collapse transition in the adsorbed phase. That is the reason why it is located at a lower temperature than in the desorbed phase.

Recognition

The recognition transition can be clearly identified for values of $a > 5.6$. The ground state is again a one dimensional chain laying completely along a stripe with $n_{\rm s} = 0, n_{\rm str} = 15, n_{\rm m} = 0$ as can be seen in Figure 3.19.

Estimating the position of the recognition transition at low temperatures

Knowing the structure of the SAW at low temperatures for different values of a makes it easy to estimate the positions of several transitions:

- solving $E(6,3,11) - E(4,4,11) = 0$ for a gives $a = 2$
- solving $E(4,4,11) - E(0,15,0) = 0$ for a gives $a = 59/11 \approx 5.4$

Microcanonical Analysis

As one can see in Figure 3.20a, the interpretation of the data from the microcanonical analysis is a bit tricky, since there are a lot of horizontal lines in the desorbed phase. Using the same rule of thumb $|E_i - E_j| > b$ removes these effects and produces the nice phase diagram in Figure 3.20b. What is left after filtering the effects of the free chain is the adsorption, recognition and the freezing ($T \approx 3.1$) transition lines. The collapse transition is not present because it is not of first-order. One can also clearly see that the slopes change at a point where two lines cross. The temperature of the recognition transition for $a > 7$ can again be trivially calculated as in section 3.4.1. The transition is between the same two types of conformations with energies $E_1 = E(0,N,0)$ and $E_2 = E(2,N-2,1)$. The transition temperature is then $T = (2a-7)/\log(28)$. The slope of the recognition transition for $a < 7$ cannot be deduced in a trivial way, since it involves different types of conformations over the range of values of a. A simple approximation for the temperature of the recognition transition in that part of the phase diagram is the transition between the conformations with energy E_1 and the type of conformations depicted in Figure 3.17 with energy $E_3 = E(4,4,11)$. The number of conformations $\Omega(E_3)$ has not been calculated explicitly but can be estimated from the density of states for $a = 6$, where $\Omega(E_3) = 11388$. Thus, the resulting transition temperature is $T = (11a-59)/\log(5694)$ and fits approximately the data points in the phase diagram.

3.4.3 The effect of z_{w}

Increasing the distance z_{w} between the bounding walls increases the volume of the systems. This results in an increase of the entropy in the high energy region, see Figure 3.21. Consequently, this leads to an increase of the slope of the straight line indicating the first order phase transition in the microcanonical entropy, which means that the adsorption temperature shifts to lower temperatures for larger values of z_{w}. This effect can be seen in the

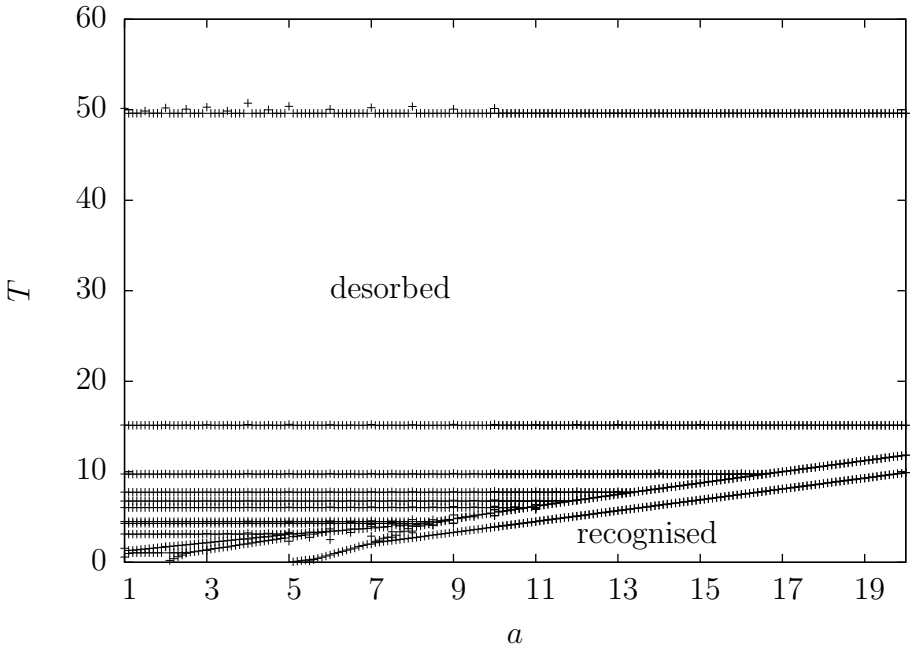

(a) $|E_i - E_j| > 0$

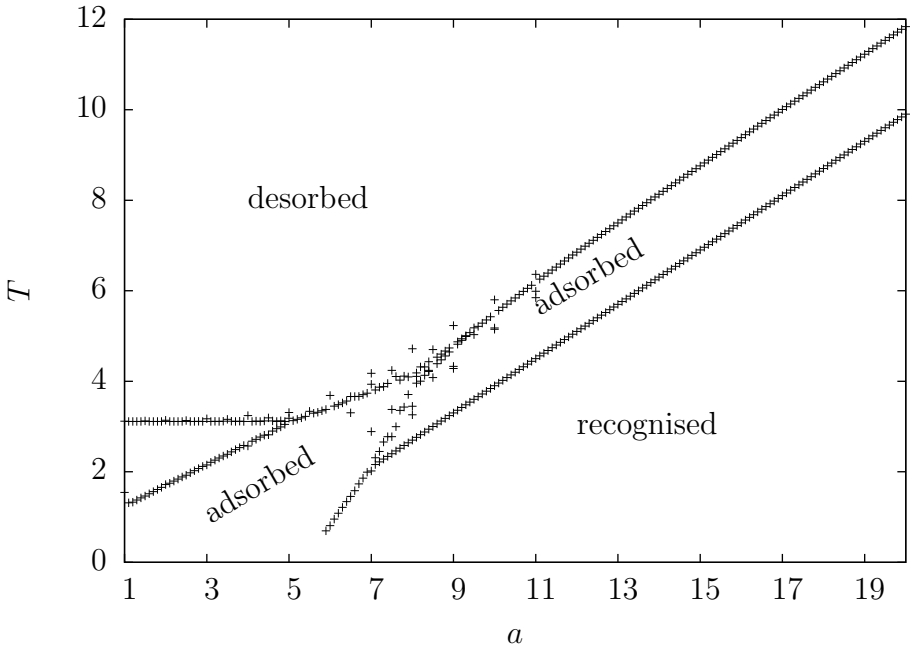

(b) $|E_i - E_j| > 5$

Figure 3.20: The phase diagram recovered from the microcanonical analysis for two different variations of the method described in 3.4.2: one allowing $|\min(E_i - E_j)| > 0$ (a) and the other allowing $|E_i - E_j| > 5$ (b). The points indicate transition temperatures computed from the density of states for different values of a for $b = 5$.

canonical phase diagram in Figure 3.22, where some of the transition lines are plotted. The decrease of the adsorption temperature allows one to clearly detect the straight horizontal line of the collapse transition in $\mathrm{d}\langle R^2_{\mathrm{gyr}}\rangle/\mathrm{d}T$ and $\mathrm{d}\langle R^2_{\mathrm{ee}}\rangle/\mathrm{d}T$ over a larger range of temperatures. One sees that as z_{w} increases, the entropy from the desorbed phase leads to larger contributions and thus the curvature in the straight line of the collapse sets on for larger values of T. This is also a good example to show that this curvature is purely a mathematical effect. The only physical information that it carries is the temperature at which the presence of the attractive surface and stripes can be detected in the desorbed phase. The same mathematical effect appears in the freezing transition line, but has been omitted from the plot for clarity.

This part of the canonical phase diagram shows another interesting effect - the adsorption transition line gets closer to the recognition transition line as z_{w} increases. These transitions cannot be clearly distinguished from each other for larger values of a in all observables that are of interest. Moreover, the transition lines for $z_{\mathrm{w}} \in \{16N+1, 32N+1, 64N+1\}$ cannot be distinguished from each other on the scale of the plot. The latter can be easily understood from the microcanonical entropy in Figure 3.21. Note that the density of states for weak self-attraction ($b = 1$) is plotted in order to make it visually clear for the reader to understand what is to follow, since the structure of the density of states in the case of strong self-attraction ($b = 5$) is more complicated, still the same arguments apply in that case too. Without loss of generality, I will drop the indices ij used in 3.4.1 and denote with $f(E) = a + bE$ the straight line passing through the points (E_1, y_1) and (E_2, y_2) of the microcanonical entropy $y(E) = \log \Omega(E)$, where $E_1 < E_2$, i.e. E_2 is the energy from the high energy region dominated by desorbed conformations. The transition temperature is then $T = 1/b$, where $b = dy/dE$ with $dy = y_2 - y_1$ and $dE = E_2 - E_1$. To a first approximation $\Omega(E_2) \propto z_{\mathrm{w}}$. It follows that in that region $y_2 \propto \log z_{\mathrm{w}}$. Since y_1 is the number of adsorbed conformations, it is constant and does not change for $z_{\mathrm{w}} \geq 2N + 1$. Thus $dy \propto \log z_{\mathrm{w}} \Rightarrow T \propto dE/\log z_{\mathrm{w}}$. Increasing z_{w} lifts the bell shaped high energy region of the entropy retaining the shape, which results in $dE \approx$ const for $z_{\mathrm{w}} \in [2N+1; 64N+1]$. Therefore, to a first approximation $T \propto 1/\log z_{\mathrm{w}}$ explains the behaviour of the adsorption transition line and also proves the intuitive result $\lim_{z_{\mathrm{w}}\to\infty} T = 0$, i.e. no adsorption for an infinitely large volume.

A better approximation in order to fit the data points is $\Omega(E_2) = pz_{\mathrm{w}} + q$, where p is the number of free conformations per starting point $\times d$ and q accounts for the number of conformations with starting points $z \leq N$ from

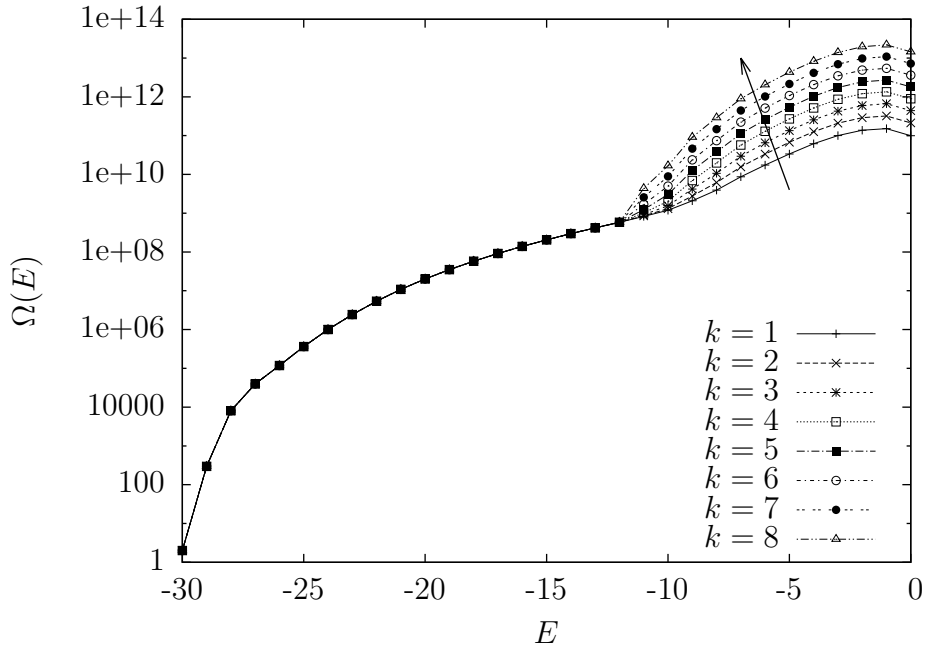

Figure 3.21: The density of states for $a = 2$, $b = 1$ and $z_w = 2^k N + 1$, with $k = 1, 2, \ldots, 8$. The arrow indicates increasing values of z_w.

a wall. The adsorption temperature in this case is

$$T \approx \frac{dE}{\log(pz_w + q) - y_1} = \frac{dE}{\log(z_w + \frac{q}{p}) + \log p - y_1}, \tag{3.7}$$

rewriting with $c_1 = dE$, $c_2 = \log p - y_1$ and $c_3 = q/p$:

$$T \approx \frac{c_1}{c_2 + \log(z_w + c_3)}. \tag{3.8}$$

The latter formula fits the simulation data acquired from the microcanonical analysis quite well for $z_w = 2^k N + 1$, with $k = 1, 2, \ldots, 8$C=. Fitted curves and the corresponding fit parameters can be found in the Appendix.

There is another misleading effect in the canonical phase diagram in Figure 3.22, namely that the recognition transition moves to higher temperatures with increasing z_w. Looking at the microcanonical phase diagram, the situation looks different - the recognition transition stays in place, it is just the adsorption transition that shifts to lower temperatures with increasing z_w. Moreover, other effects appear for large values of a: the slope of the adsorption transition decreases with increasing z_w. Eventually, for large enough z_w the adsorption transition merges with the recognition transition as illus-

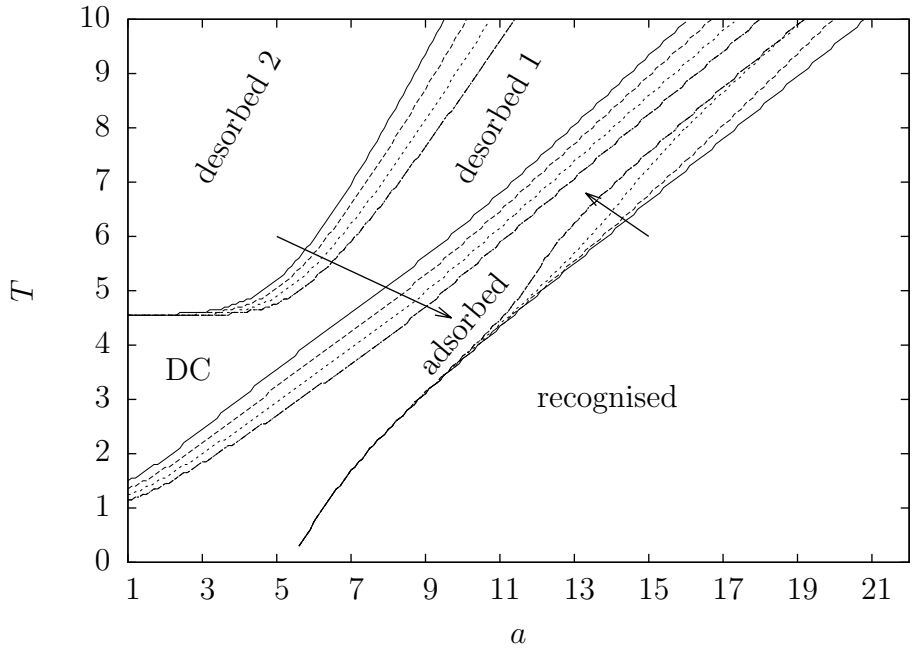

Figure 3.22: Part of the canonical phase diagram for $b = 5$ and $z_w = 2^k N + 1$, with $k = 1, 2, \ldots, 6$. The arrows indicate increasing values of z_w on each transition line. Note that the curves for $k \geq 4$ cannot be distinguished from each other on this scale.

trated in the microcanonical phase diagram for $z_w = 128N + 1$ in Figure 3.23. Further increase of z_w results in a shift of the merged transition to lower temperatures. The merge of the adsorption and the recognition transitions can be easily explained by the fact that the high temperature regime is dominated by the entropy of the free chain, where the low temperature regime is dominated by the high Boltzmann weight of the recognised chain. In other words, an adsorbed but not recognised chain has low entropy and low Boltzmann weight and plays a less significant role in the ensemble averages with increasing values of a and z_w.

3.4.4 Wider stripes ($w = 2, d = 5$)

Exact enumeration has been done also on a system with larger stripe width. The value chosen here is $w = 2$. The distance between the left-most edges of neighbouring stripes is kept fixed at $d = 5$. The overall system behaviour is similar. One finds the same types of phases and phase boundaries. The main difference here is that the increased stripe width increases the fraction

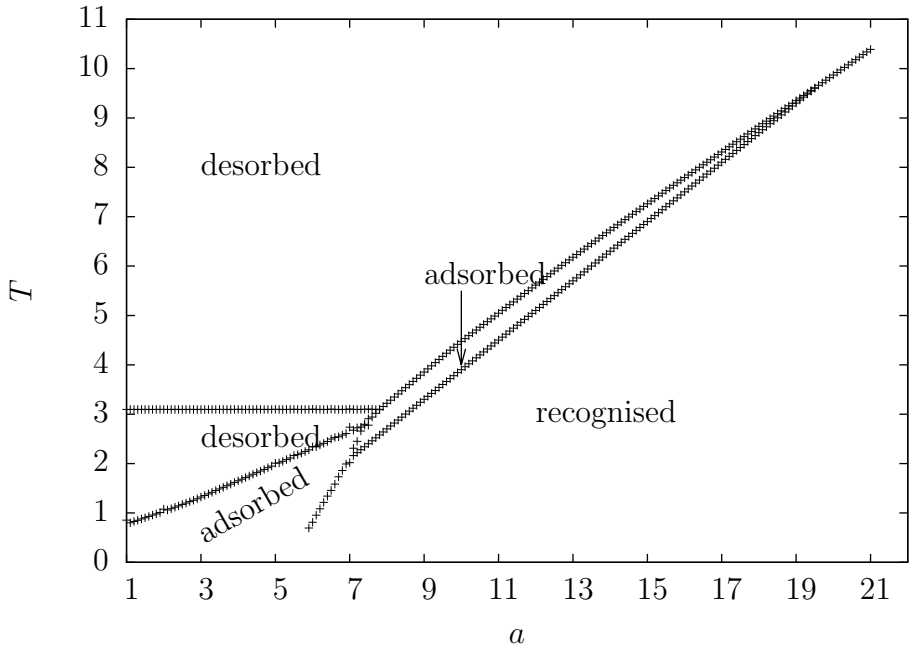

Figure 3.23: The microcanonical phase diagram for $b = 5$ and $z_w = 128N + 1$ using the filtering criteria $|E_i - E_j| > b$.

of the surface covered by the stripes from 1/5 for $w = 1$ to 2/5 for $w = 2$. This changes the ground states in the different phases and results in shifts of the phase boundaries. The phase diagrams for weak ($b = 1$) and strong ($b = 5$) self-attraction are plotted in Figures 3.24 and 3.25.

Adsorption transition

The increased fraction of the stripe surface allows the chain to be adsorbed easier for values of $a > 1$. This explains the increase of the slope of the transition line. The ground states in the "adsorbed" phase are different from the ones in the system with narrow stripes, but that does not affect the overall structure of the phase diagram.

Recognition transition

An important difference here is the fact that the wider stripes change the ground state of the recognised chain. In this case, the linear chain structure is no longer the one with the lowest energy. The wider stripe makes it possible for the chain to create self-contacts without the loss of stripe contacts. This results in conformations with lower energies compared to the system with

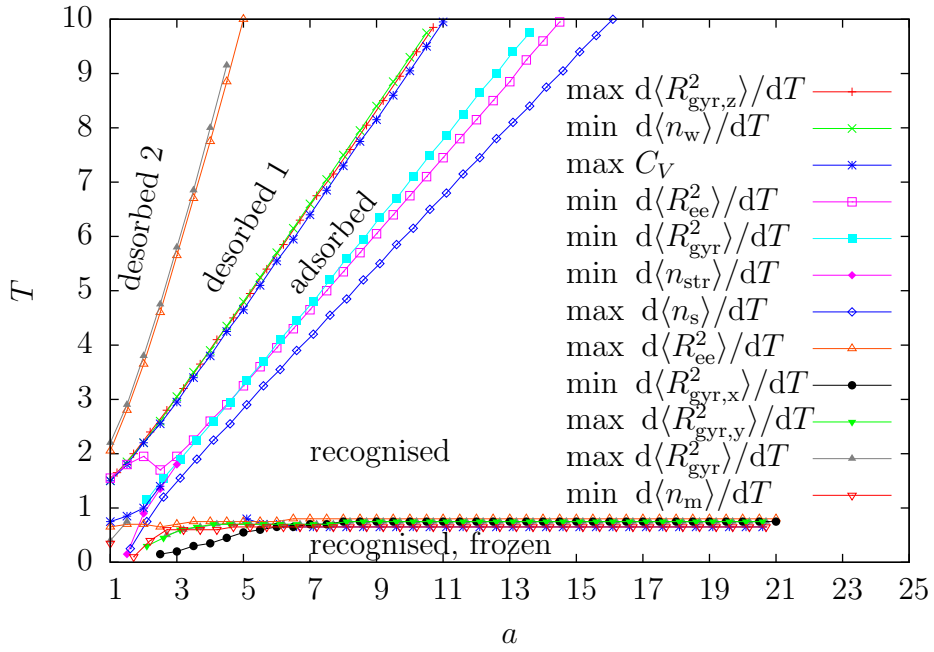

(a)

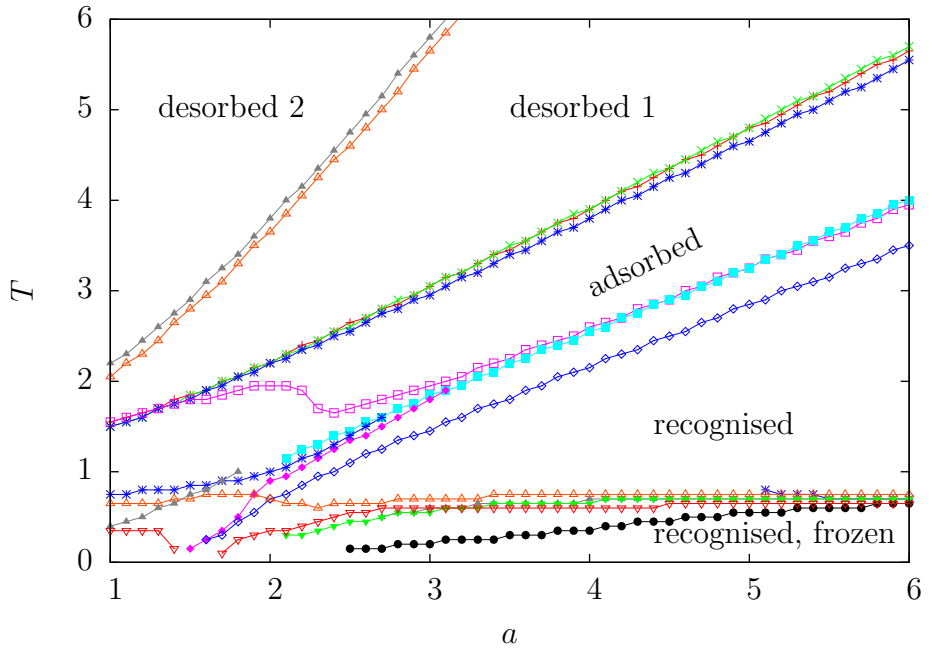

(b)

Figure 3.24: (a) the phase diagram of the system with $b = 1$ (b) a zoom-in of the interesting part of the plot. The curves indicate minima or maxima of d⟨$\mathcal{O}$⟩/dT for different values of the monomer-stripe interaction a. The legend of (b) is the same as that of (a), every 5th data point is plotted in (a). (Note that the data set is up to $a = 21$ but the plot has been extended to accommodate the legend.)

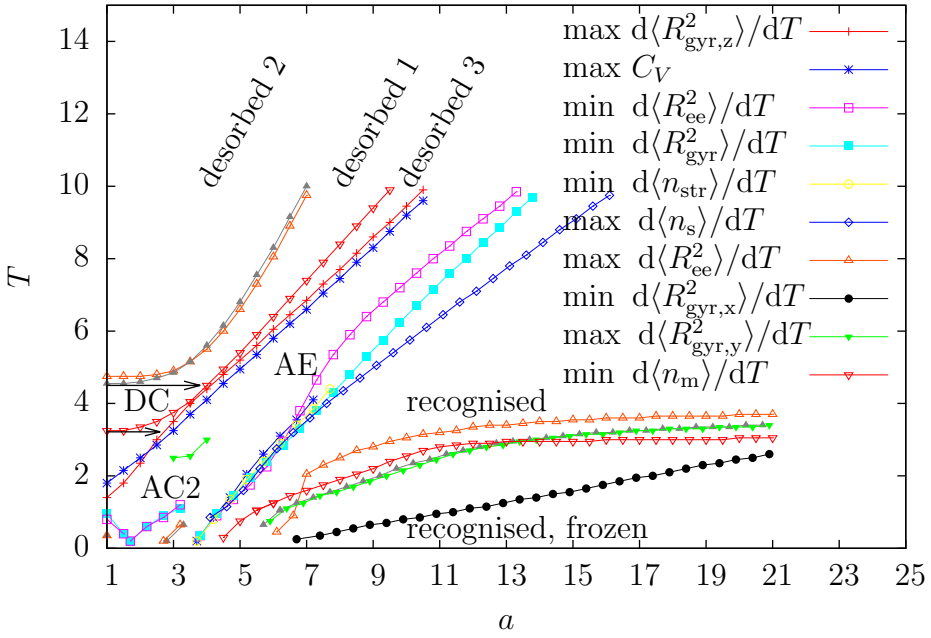

(a)

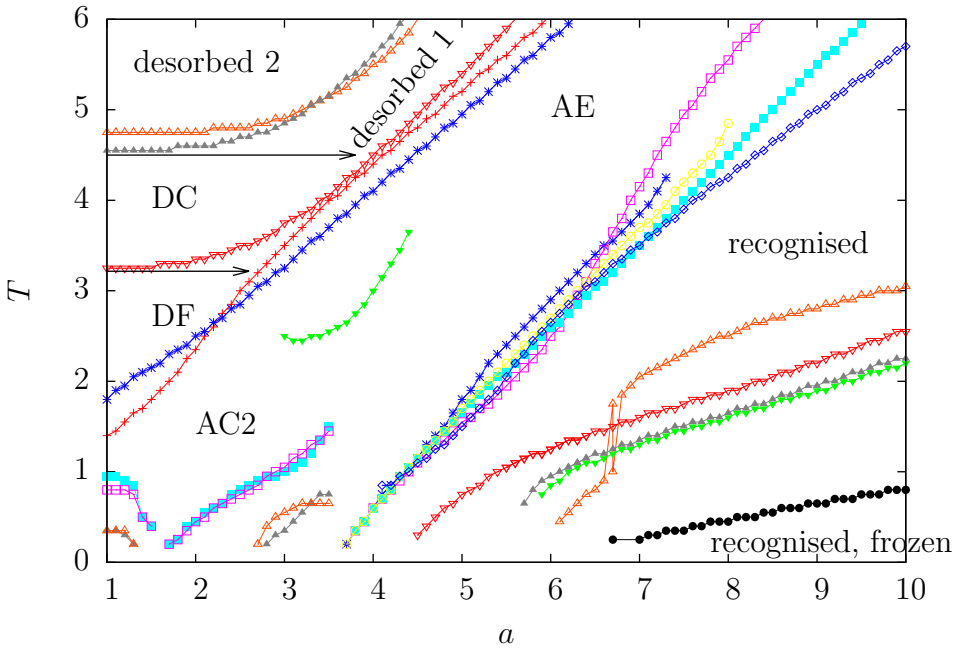

(b)

Figure 3.25: (a) the phase diagram of the system with $b = 5$ (b) a zoom-in of the interesting part of the plot. The curves indicate minima or maxima of d⟨$\mathcal{O}$⟩/dT for different values of the monomer-stripe interaction a. The legend of (b) is the same as that of (a), every 5th data point is plotted in (a). (Note that the data set is up to $a = 21$ and $T = 10$ but the plot has been extended to accommodate the legend.)

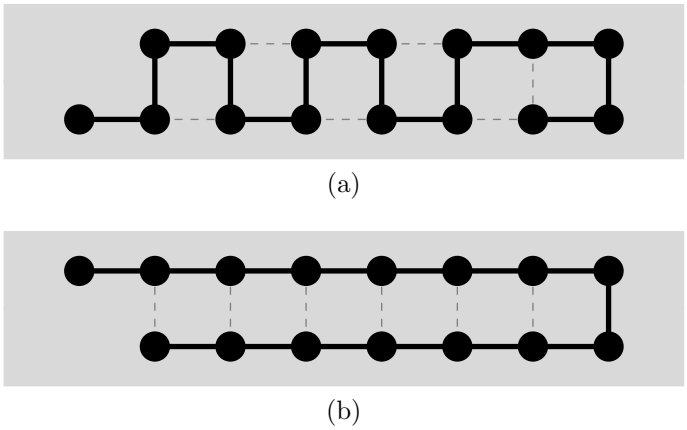

Figure 3.26: Example ground states for large values of a of the system with wider stripes. Both conformations (a) and (b) have the same energy.

narrow stripes. Moreover the ground state in the recognised phase is highly degenerate. It is a SAW confined on a stripe with maximum self-contacts as illustrated in Figure 3.26, where two possible conformations are depicted. Contrary to the narrow stripe system, there are some temperature induced effects in this part of the phase diagram. Increasing the temperature leads to breaking some self-contacts, thus stretching the chain along the stripe. This could also be related to the freezing transition, since it is dependent only on the strength of the self-interaction b. Hence happens at constant temperature $T_{rfreezing}$ for large values of a. Moreover, $T_{rfreezing} \approx 0.65$ for $b = 1$ is close to the temperature where the freezing transition of the free chain takes place. Increasing b results in a linear shift of $T_{rfreezing}$ as in the case of the freezing transition temperature. The part of the "recognised" phase where the frozen conformations dominate is denoted here as the "recognised,frozen" phase and the boundary between both is indicated by the approximately horizontal line in the bottom part of the phase diagram. The slope of the recognition transition line (the one separating the "adsorbed" and the "recognised" phases) is greater than in the system with narrow stripes again due to the larger fraction of the wall, which is occupied by the stripes.

Collapse transition

The collapse transition should be located below the adsorption transition for $b = 1$ and cannot be clearly identified. For larger self-attraction ($b = 5$) it is located above the adsorption transition for small values of a and can be detected on the canonical phase diagram. Moreover, in this case the collapse in the "adsorbed" phase is poorly detectable as peaks in the

canonical expectation values of the observables considered. There is only one curve that approximately indicates the collapse and hence the boundary between the "AE" and "AC2" phases. The influence of the attractive surface on the desorbed phase is again indicated as the line separating the "desorbed 1" and "desorbed 2" phases.

Freezing transition

The freezing transition is located below the adsorption transition for $b = 1$ and is not clearly identifiable as well. For larger self-attraction ($b = 5$) it is located above the adsorption transition for small values of a. The influence of the attractive surface on the desorbed phase is also indicated by bending of the curve upwards and the part of the phase diagram that I have labelled as "desorbed 3".

Microcanonical analysis

The microcanonical phase diagram of the system with wider stripes is more complicated due to the fact that the wider stripes allow several transitions between two-dimensional conformations fully attached to a stripe but with different number of self-contacts. These can be identified as horizontal lines in the recognised phase. Moreover, the transition between the "recognised" and the "recognised,frozen" phases is also detected using the microcanonical analysis. The conformations from both phases have neighbouring energies E_1 and E_2 where $|E_1 - E_2| = b$. Due to this, the transition line gets filtered when using the criteria $|E_i - E_j| > b$ to obtain the most important parts of the phase diagram, see Figures 3.27 and 3.28. However, a horizontal line in the recognised phase passes this criteria, but that one is not associated with the transition between the "recognised" and the "recognised,frozen" phases.

Another peculiar fact is that the part of the "adsorbed" phase not containing the "recognised" phase disappears when the self-attraction is stronger ($b = 5$) for larger values of a and one observes a direct transition between the "desorbed" and the "recognised" phases in that parameter range, though the canonical phase diagram indicates what seems to be two separate transitions. This, however, can be misleading since for $N = 19$ one can clearly detect two separate lines in the microcanonical phase diagram in Figure 3.29 indicating the adsorption and the recognition transitions.

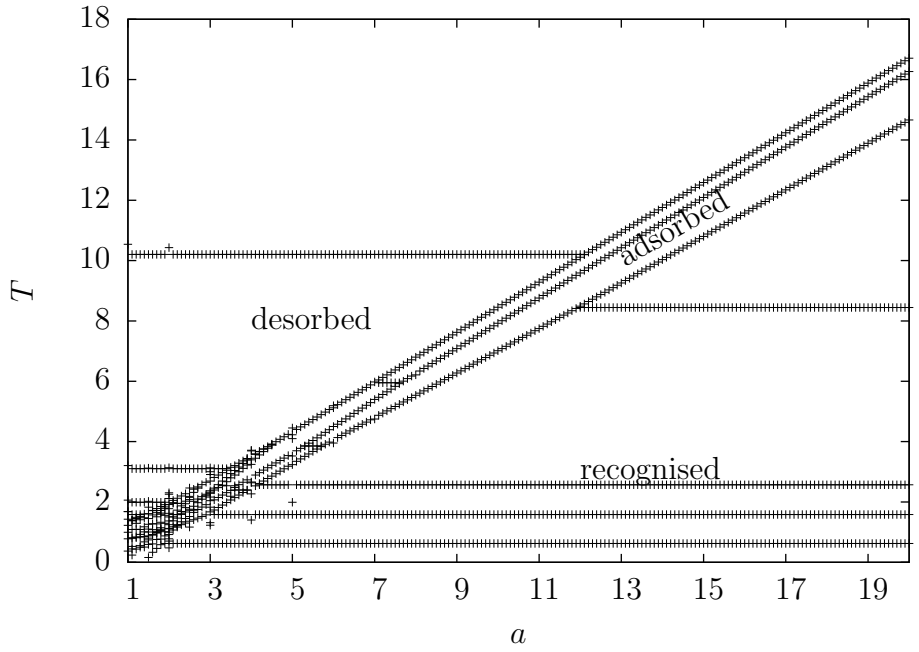

(a) $|E_i - E_j| > 0$

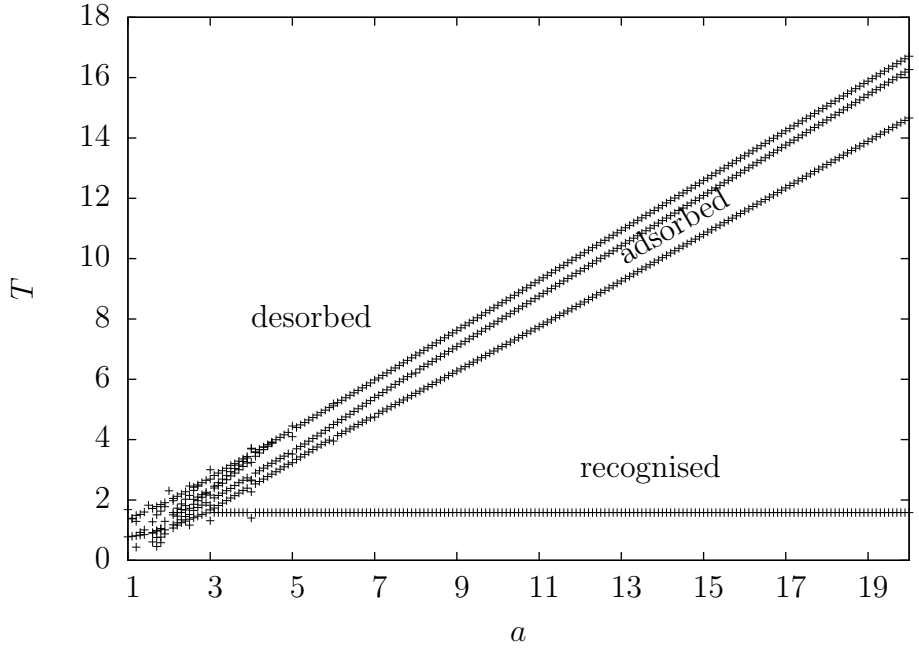

(b) $|E_i - E_j| > b$

Figure 3.27: The phase diagram recovered from the microcanonical analysis for two different variations of the method described in 3.4.1: one allowing $|\min(E_i - E_j)| > 0$ (a) and the other allowing $|E_i - E_j| > b$ (b). The points indicate transition temperatures computed from the density of states for different values of a for $b = 1$.

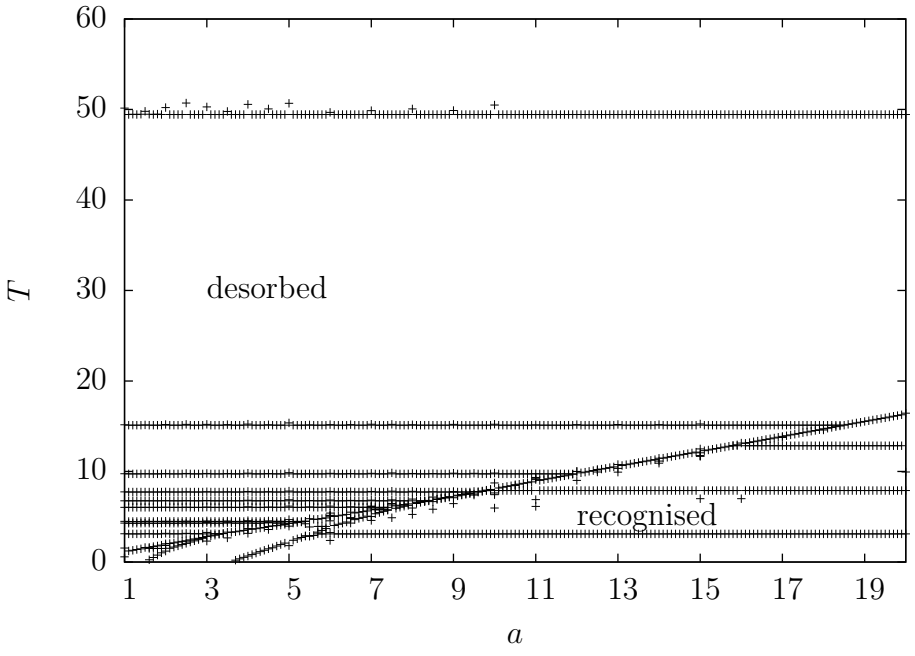

(a) $|E_i - E_j| > 0$

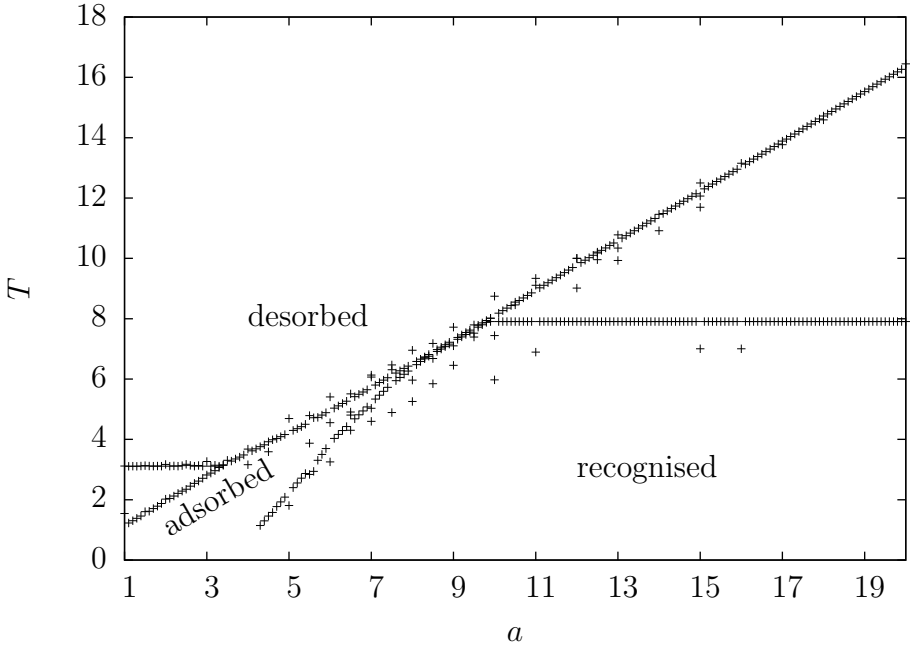

(b) $|E_i - E_j| > b$

Figure 3.28: The same as in Figure 3.27 but for $b = 5$.

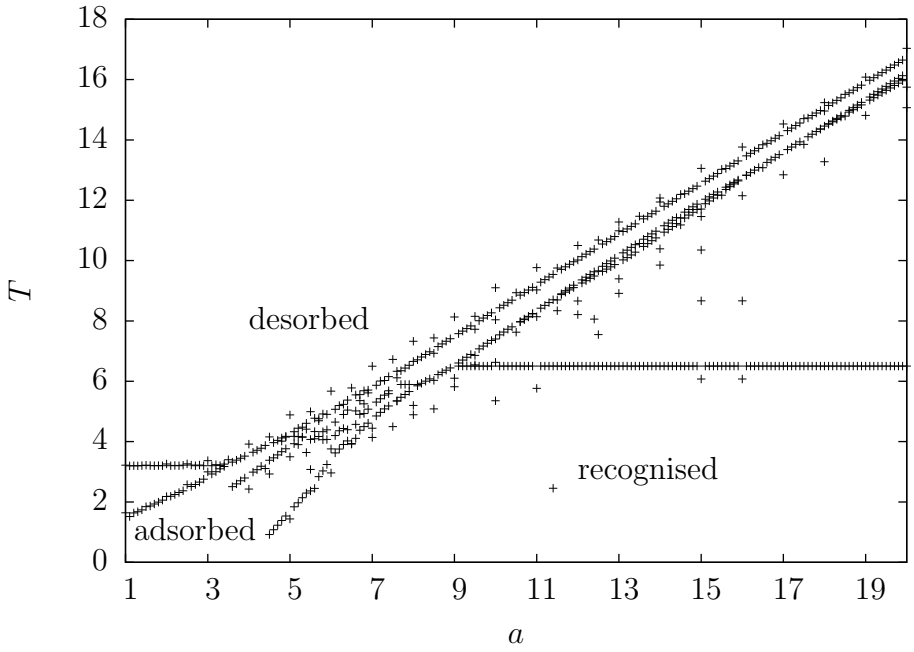

Figure 3.29: The computed microcanonical phase diagram for $N = 19$, $b = 5$ using the filtering criteria $|E_i - E_j| > b$.

3.5 Chain in a cavity ($N = 15, 16, 17, 18, 19$)

3.5.1 Narrow stripes ($b = 1, w = 1$)

The overall structure of the phase diagram does not change in the range $15 \leq N \leq 19$. The main difference is that the adsorption and recognition transition lines in the canonical phase diagram shift to higher temperatures. The shift is greater for larger values of a. The adsorption transition shifts more than the recognition transition, which is barely detectable on the scale of the plot in Figure 3.30. However, the microcanonical plot in the same Figure shows a different behaviour. The adsorption transition shifts to higher temperatures with increasing chain length, but the recognition transition shifts to lower temperatures.

3.5.2 Narrow stripes and stronger self-attraction ($b = 5, w = 1$)

The overall structure of the phase diagram of the system with narrow stripes and stronger self-attraction does not change for $15 \leq N \leq 19$. The directions

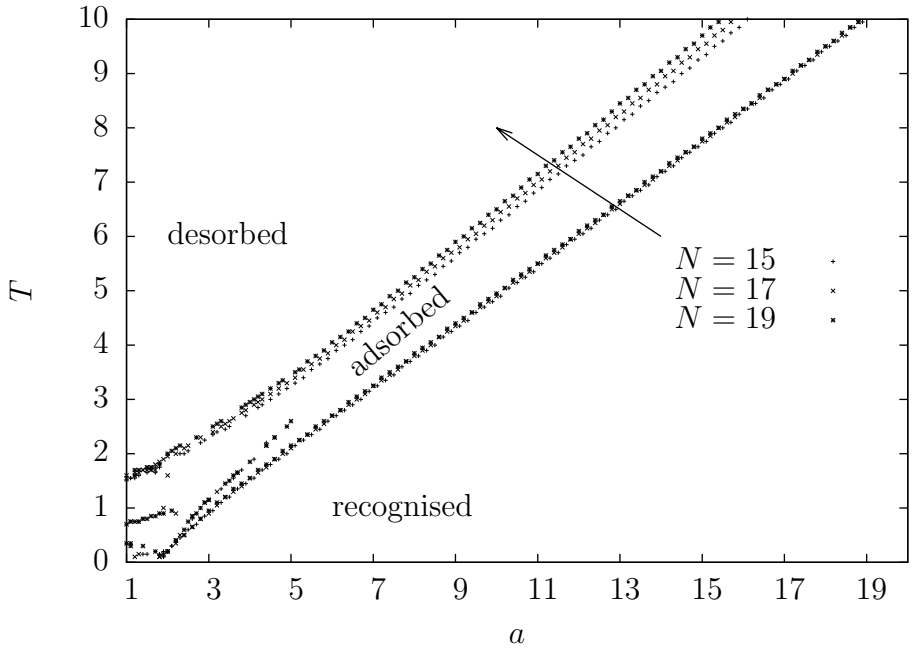

(a) canonical

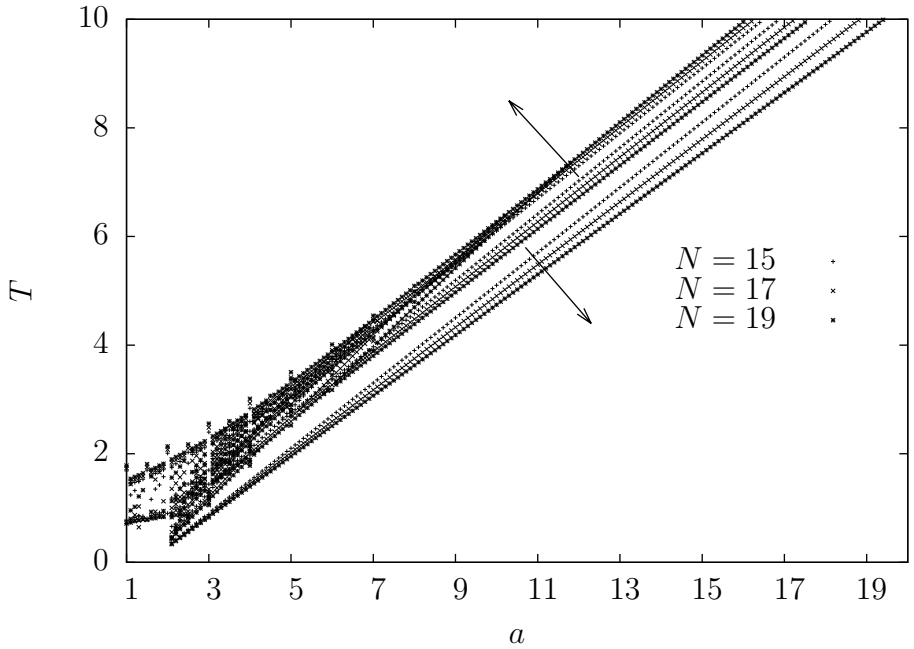

(b) microcanonical $|E_i - E_j| > b$

Figure 3.30: (a) part of the canonical phase diagram for $b = 1$ for $15 \leq N \leq 19$, (b). The arrows indicate increasing values of N. Note that every 2nd data point has been plotted in (a).

of the shifts in the transitions are the same as in the case of weak self-attraction ($b = 1$).

3.5.3 Wider stripes $w = 2$

The overall structure of the phase diagram of the system with wider stripes does not change for $15 \leq N \leq 19$. The directions of the shifts in the transitions are the same as in the case of narrow stripes both for $b = 1$ and $b = 5$.

3.6 Chain in a cavity - comparison to Monika Möddel's results

Monika Möddel has studied a similar model as part of her PhD Thesis [12] at the University of Leipzig. Her work is based on Monte Carlo computer simulations of polymer chains in continuum, i.e. the positions of the monomers are not confined to a lattice. The self-attraction, self-repulsion (analog to the self-avoidance on lattice) and the wall attraction have been modelled by continuous potentials. The chain length is chosen to be $N = 40$. One cannot do a simple one-to-one mapping between the results in that work and the present work. The choice of the chain length affects the absolute positions of the collapse and freezing transitions of the free chain. The choice of the lattice (continuum in Möddel's work) affects the number of nearest neighbours, the maximum number of self-contacts for a fixed chain length N, as well as geometry of preferable conformations. This might also affect the absolute position of the collapse and freezing transitions as well. The position of both is also affected by the chosen strength of the self-attraction. These facts alone, do not allow a simple one-to-one mapping between both works. However, qualitatively the results of both works are comparable in terms of the stripe-attraction vs. temperature phase diagrams:

- the general structure of the phase diagram is similar - the phases appear in the same order, the phase boundaries have comparable shapes
- the slope of the adsorption transition increases with increasing stripe width
- a freezing transition can be found in the "recognised" phase of the system with wider stripes and none could be found in the case of narrow stripes

- the collapse transition could be located in the "adsorbed" phase at lower temperatures than the collapse transition in the "desorbed" phase.
- the "width" of the transitions lines in Möddel's work has been indicated in this work by plotting the peaks of several observables (where possible), in order to show that there is a certain "spread" of the signal in these finite systems

Quantitatively, the results are not comparable, but the interesting part of the phase diagram is located at temperatures and stripe attractions of the same order of magnitude: $1 \leq a \leq 10$, $0 \leq T \leq 10$.

3.7 Chain grafted to a stripe

3.7.1 $N = 15, w = 1, d = 5, b = 1$

This section considers a grafted chain, i.e. one end of the ISAW is fixed to a stripe. The chain is allowed to extend completely, i.e. $z_{\mathrm{w}} > N$. The latter is equivalent to removing the steric wall, since the chain cannot enter the free space with coordinate $z > N$ and hence that part of the volume has no contribution to the system and can effectively be removed. The lack of free chains results in reduced entropy in the high energy region. This effect can be seen by comparing the the density of states of the grafted and the non-grafted systems, which are plotted in Figures 3.31 and 3.10a, respectively.

The high energy region, where the entropy reduction takes place is $E >= -11$ for this chain length. This results in a change of the adsorption transition, since the convex intruder is not present any more. Due to the grafting of the chain, at least one monomer is attached to a stripe at all times. Therefore globular conformations cannot be adsorbed by creating arbitrary contacts with the wall, since one end of the chain must have a contact with a stripe.

The entropy in the low energy region has similar structure in both cases. This indicates that the recognition transition is similar in both systems. However, the degeneracy of the $E(2, N-2, 1)$ state is lower than in the non-grafted system, because some of the conformations where one end of the chain is not on the stripe are not allowed (see Figure 3.13 for an illustration). Therefore, the slope of the recognition transition in the microcanonical analysis is higher $T = (2a-3)/\log(26)$, compared with $T = (2a-3)/\log(28)$ for the non-grafted system.

The adsorption transition in this system can be detected only as a minima in $\mathrm{d}\langle n_{\mathrm{w}}\rangle/\mathrm{d}T$ and $\mathrm{d}\langle R^2_{\mathrm{gyr,z}}\rangle/\mathrm{d}T$ for larger values of a. For small a, one can

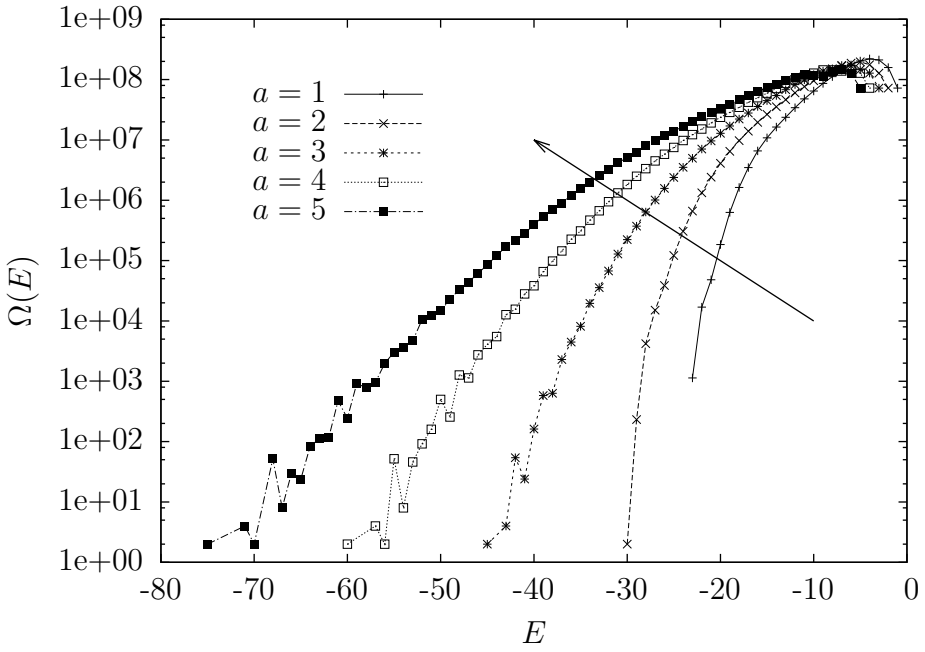

Figure 3.31: The density of states of the grafted system for integer values of a. The arrow indicates increasing value of a.

detect a maxima in C_V and a minima in $\mathrm{d}\langle \mathcal{O} n_{\mathrm{str}} \rangle / \mathrm{d}T$, but the peaks from the recognition transition are much higher and the trace of the adsorption transition disappears in these observables as can be seen in Figure 3.32. The peaks in C_V and $\mathrm{d}\langle \mathcal{O} n_{\mathrm{str}} \rangle / \mathrm{d}T$ indicating the adsorption transition are approximately at the position of the signal in $\mathrm{d}\langle n_{\mathrm{w}} \rangle / \mathrm{d}T$ for small a, but the the signal in $\mathrm{d}\langle R^2_{\mathrm{gyr,z}} \rangle / \mathrm{d}T$ deviates from that.

Surprisingly, the microcanonical phase diagram in Figure 3.33 is rich on information on in what could be labelled here as the "desorbed" phase. However, analysing all of the is not in the scope of this work. The recognition transition line can be analytically calculated as was mentioned before, but one cannot clearly identify the adsorption transition curve.

3.7.2 $N = 15, w = 2, d = 5, b = 1$

Increasing the stripe width to $w = 2$ accounts for the appearance of the "recognised,frozen" transition as in the case of the non-grafted system. This can be seen in the phase diagram in Figure 3.34. The slopes of the recognition transition and the indications for the adsorption transition are larger, as in the case of the non-grafted system. This is expected, since the stripes

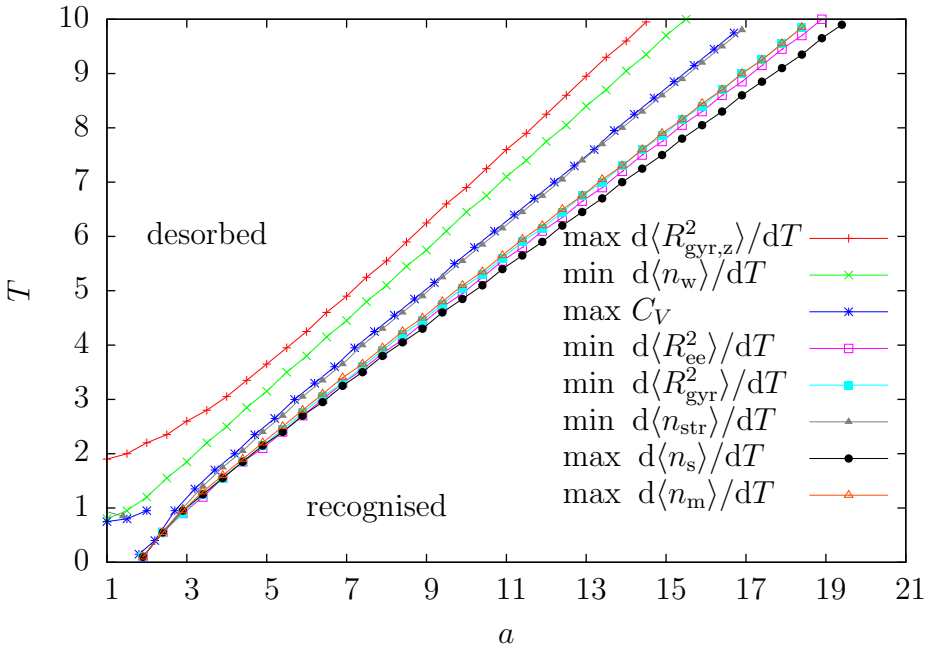

(a)

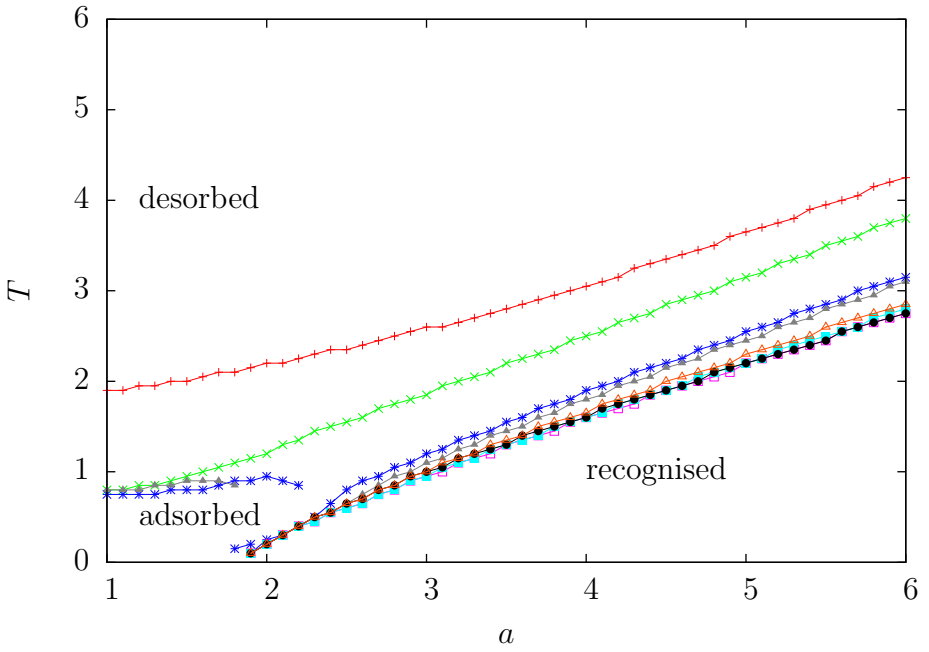

(b)

Figure 3.32: (a) the phase diagram of the system with (b) a zoom-in of the interesting part of the plot. The curves indicate minima or maxima of d⟨$\mathcal{O}$⟩/dT for different values of the monomer-stripe interaction a. The legend of (b) is the same as that of (a), every 5th data point is plotted in (a).

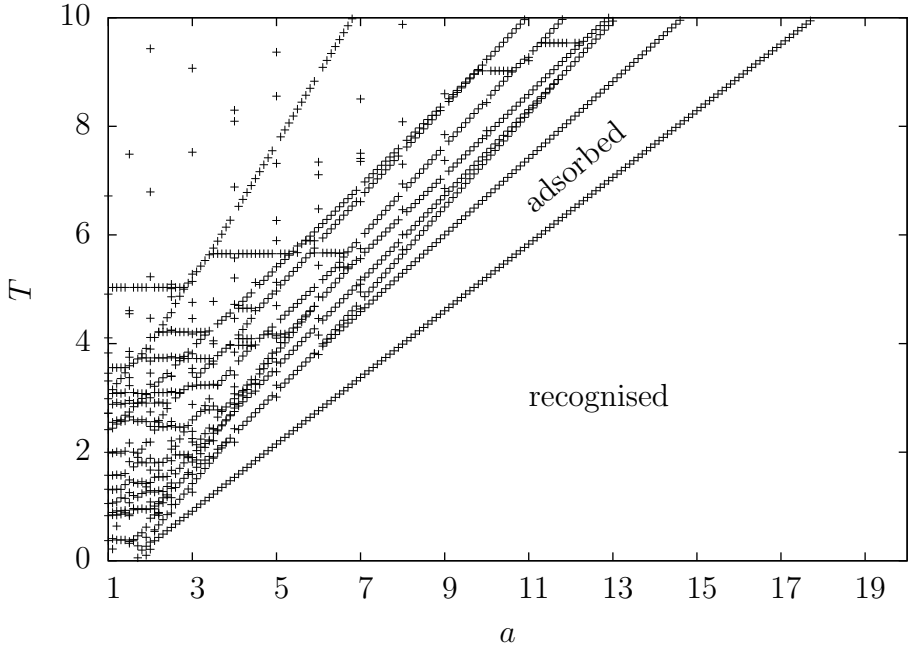

(a) $|E_i - E_j| > 0$

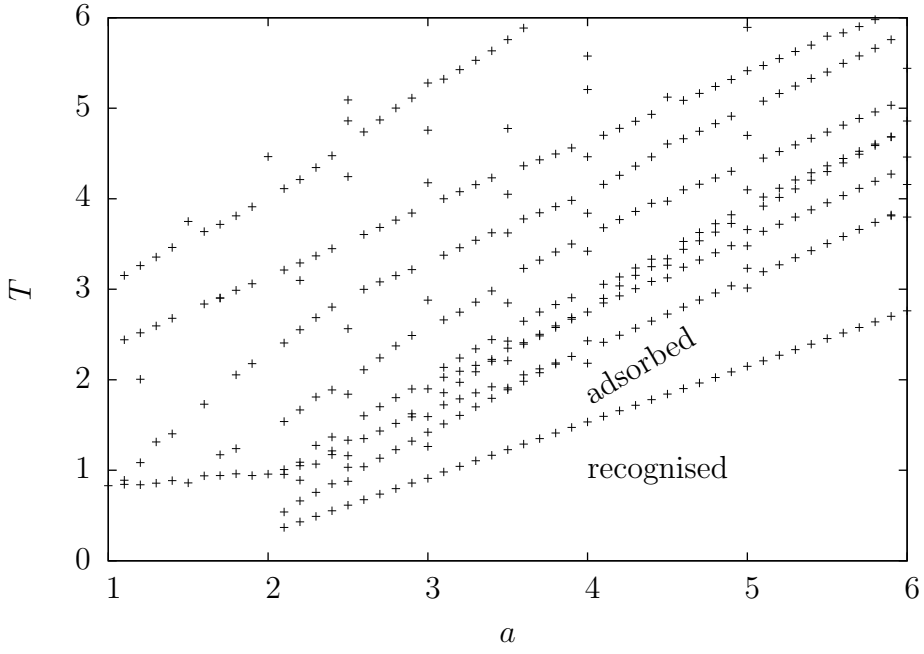

(b) $|E_i - E_j| > b$

Figure 3.33: (a) part of the computed microcanonical phase diagram of the system; (b) a zoom-in of the interesting part of (a).

occupy a larger fraction of the surface and thus allow for easier adsorption of the chain. The microcanonical diagram is skipped here. It shows again transition lines at constant temperatures in the recognised phase as in the case of non-grafted system. The transition between the "recongised" and the "recognised,frozen" phases is again detected in the microcanonical analysis and is hence a first-order phase transition. The part of the microcanonical phase diagram where the desorbed phase it located is again rich of detected transitions. These are, as already mentioned, not in the scope of this work.

3.7.3 $N = 15 - 19$, stronger self-attraction

One can force the grafted chain to undergo a collapse transition in the desorbed phase by increasing the strength of the self-interaction. The parts of the chain no connected to the surface allow for comparable effects to the free chain, i.e. a collapse and freezing transitions can be detected. The location of the transition temperatures for both are close to the ones of the free chain. The effect of increasing b is again an approximately linear shift of both the collapse and the freezing transitions. Moreover, because of these similarities to the non-grafted system, further discussion will be skipped.

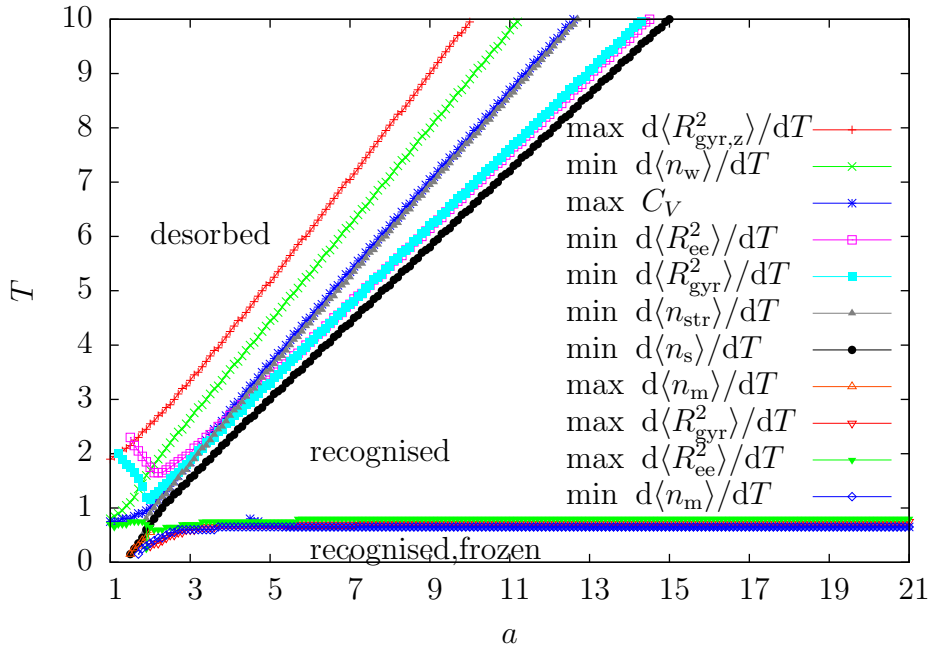

(a)

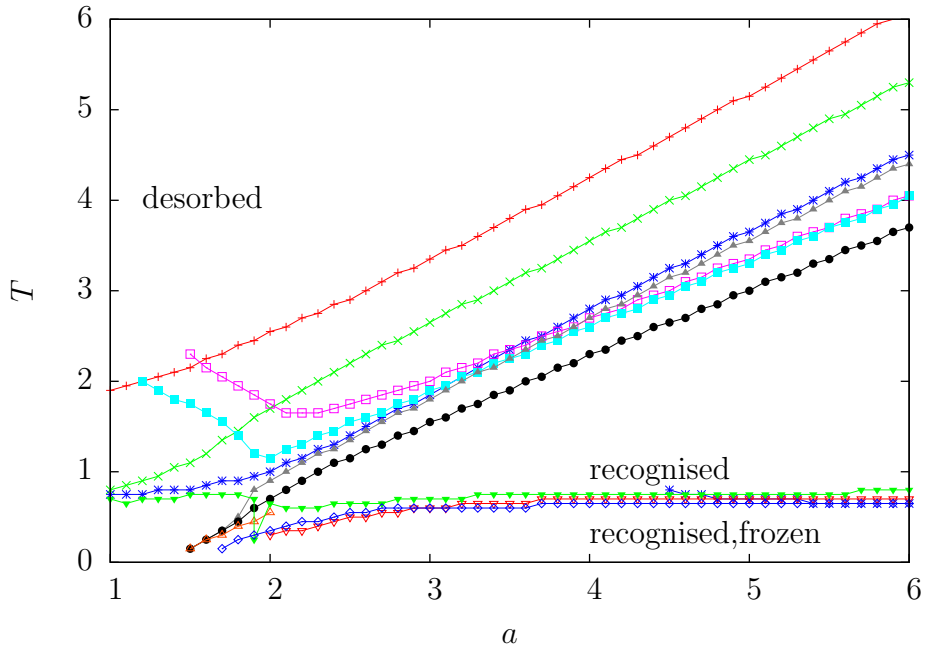

(b)

Figure 3.34: (a) the phase diagram of the system with (b) a zoom-in of the interesting part of the plot. The curves indicate minima or maxima of d⟨$\mathcal{O}$⟩/dT for different values of the monomer-stripe interaction a. The legend of (b) is the same as that of (a), every 5th data point is plotted in (a).

Chapter 4

Pruned-Enriched Rosenbluth Method

4.1 Introduction

There are a few disadvantages when using the method of exact enumeration:

- one cannot enumerate large systems in a reasonable amount of computer time
- one obtains only statistical averages of the observables and loses the detailed information about the typical conformations for each phase.

The first one is a major disadvantage when one wants to obtain information about larger systems or is interested in scaling behaviour. The second one is a major disadvantage when it comes to studying the geometrical shapes that the ISAW forms in the different phases. The exact enumeration delivers statistical averages but one cannot ask questions such as: what is the typical shape a certain part of the phase diagram. One can read off the expected values of certain observables like different types of contact numbers or the chain energy. But when one wants to study a conformation specified by these parameters, one needs to re-enumerate the whole system again and save out the chains of interest. Repeating this step several times for each phase is a highly impractical approach since the enumeration takes quite a long amount of time. In order to cope with both problems one can resort to the method of Monte Carlo simulations. There are two approaches that one can choose:

- Markov chain Monte Carlo methods - one starts with a complete system, which evolves in fixed steps according to certain rules

- chain growth Monte Carlo methods - one tries to generate a complete system multiple times.

In the first method one needs a good set of rules for system evolution. In the case of lattice polymer models these rules try to move parts of the chain or cut parts of it and put them on other places. After applying the rules, which is called an update, one gets possibly a new system state, which can further be changed by doing an update again. This sampling method must satisfy two major criteria: detailed balance and ergodicity. Due to the geometrical constraints implied by the self-avoidance requirement for the chain, however, a "good" set of rules is needed. Finding such a set is not a trivial task and there has been a lot of research in this direction [23, 24, 25].

Another approach is the chain growth method. One starts at a fixed point in the system and tries to generate a chain by growing it step by step from that point. Choosing the next step is done again via a certain set of rules. The simplest one would be to try to complete the chain by choosing the next step at random. This however leads to creating conformations that do not fulfil the self-avoidance requirement. The result is a waste of computation time, since these chains are invalid, need to be discarded and one has to start growing the chain from the beginning.

The first idea to try to generate random SAWs without wasting that much computer time is relatively old an can be traced back to [6]. Their rules are quite simple: choose the next step at random from all possible valid new steps, i.e. all possibilities fulfilling the self-avoidance constraint. Each chain of length N is given a weight W_N^{RR} to correct the bias introduced by choosing only valid new steps:

$$W_N^{\mathrm{RR}} = \prod_{n=1}^{N} m_n \tag{4.1}$$

where m_n is the number of valid choices for the next step at the partial length n. The formula can also be written in a recursive form:

$$W_n^{\mathrm{RR}} = W_{n-1}^{\mathrm{RR}} m_n \tag{4.2}$$

where W_n^{RR} is the weight of the partial chain of length n. Partial chains with no possible continuation, i.e. $m_n = 0$ are given the weight $W^{\mathrm{RR}} = 0$ and are hence discarded. The expectation value of the observable $\mathcal{O}$ is computed as:

$$\langle \mathcal{O} \rangle = \frac{\sum_i \mathcal{O}_i W_i}{\sum_i W_i} \tag{4.3}$$

where $\mathcal{O}_i$ and $W_i = W_{N,i}^{\mathrm{RR}}$ are the value of the observable and the weight of the chain generated at the try i, respectively. This method might lead to biased results as a small number of chains with large weights can dominate the sum. Moreover, it is not as efficient as desired since partial chains that cannot be completed due to a dead end, i.e. $W^{\mathrm{RR}} = 0$ are a waste of computer time as they do not enter the sum. The number of full chains n_N of length N obtained from n_0 tries to grow a full chain decreases exponentially with N:

$$n_N = n_0 \exp\left(-\lambda N\right). \tag{4.4}$$

This effect is called attrition and a possible solution to it has been proposed short after in [26]. Their idea of tackling the problem is called enrichment: taking p copies of the partial chain each s steps and trying to complete all copies independently. A proper choice of p and s would reduce the effect of attrition. A bad choice would lead to biased statistics. Their criteria for a good choice is keeping the number of samples per enrichment step constant.

However, this approach does not mitigate the other problem, namely the bias in $\langle \mathcal{O} \rangle$. The latter has been tackled by a relatively new method called Pruned-Enriched Rosenbluth Method (PERM) [27]. It uses the idea of enrichment, but does not always enrich the partial chain every s steps. It rather enriches by a factor p only when its weight $W_n > W_n^{>}$, where $W_n^{>}$ is the enrichment threshold. Moreover, this method introduces a mechanism to control the number of chains with low weights: partial chains with weights $W_n < W_n^{<}$, where $W_n^{<}$ is the pruning threshold, are discarded with a certain probability q. The events of pruning and enrichment are accounted for by correcting the weight of the partial chain to account for the introduced bias: $W_n = W_n/p$ after enrichment and $W_n = W_n/q$ after pruning. This method allows one to control the distribution of the weights of the generated chains, i.e. not spending too much computational time on lots of chains with low weights. However, choosing the amount and threshold of enrichment and pruning ($p, q, W_n^{>}$ and $W_n^{<}$) is not a trivial task. Bad choices might lead to bad sampling.

Trivial choices that one can make are $p = 2$ and $q = 0.5$. The proposal for choosing $W_n^{>}$ and $W_n^{<}$ in [27] is based on the idea of dynamic self tuning of the algorithm to the running average of the partition sum $Z_n = \sum_i W_{n,i}$. Initially, one sets $W_n^{>} = \infty$ and $W_n^{<} = 0$ in order to obtain some guess of Z_n for every length $1 \leq n \leq N$. After that one sets $W_n^{>} = c^{>} Z_n/Z_1$ and $W_n^{<} = c^{<} Z_n/Z_1$ where $c^{>}$ and $c^{<}$ are constants. The article quotes good results for $c^{>}/c^{<} \approx 10$, where $c^{>}$ and $c^{<}$ are of order 1. Note that I could not find reliable, in my opinion, rules for tuning the algorithm such that one

can be sure that the resulting statistics is correct. The only "reliability test" that I could find was in [28], but that was not satisfactory for me. However, there have been newer algorithms using the idea of PERM [29, 11, 30], but they do not mention anything about the reliability of the resulting statistics.

Introducing a temperature to the system, one introduces the Boltzmann factor $\exp(-\beta E)$ to the weight. Now the Rosenbluth-Rosenbluth sampling is equivalent to a simple sampling. On every step n one chooses a free site $k \in [1, m_n]$ with the same probability $p_k = 1/m_n$. The final weight of the chain in this case is $W_N = W_N^{\mathrm{ss}}$ with:

$$W_N^{\mathrm{ss}} = W_N^{\mathrm{RR}} e^{-\beta E} = \prod_{n=1}^{N} \frac{1}{p_k} e^{-\beta E_k} = \prod_{n=1}^{N} m_n e^{-\beta E_k} \tag{4.5}$$

where E_k is the energy corresponding to the chosen next step k.

One can also do importance sampling by choosing the next site k with a probability depending on the energy contribution of that site:

$$p_k = \frac{e^{-\beta E_k}}{\sum_{k'=1}^{m_n} e^{-\beta E_{k'}}} \tag{4.6}$$

in which case the final weight of the chain becomes

$$W_N = W_N^{\mathrm{is}} = \prod_{n=1}^{N} \frac{1}{p_k} e^{-\beta E_k} = \prod_{n=1}^{N} \sum_{k'=1}^{m_n} e^{-\beta E_{k'}}. \tag{4.7}$$

Equipped with this Monte Carlo technique one can easily obtain conformations from the interesting parts of the phase diagram by running the algorithm with the desired set of parameters $(a, b, N, z_{\mathrm{w}}, T)$. The chains with desired properties, such as specific number of contacts or energy, can be easily obtained and saved for later analysis. Using a computer, one can visualise the conformation in order to analyse it's geometrical shape and properties. Using PERM, I was able to create and analyse the figures of conformations in this thesis.

One can also use this MC method to study the phase diagram of the system discussed in this thesis. One needs at least one simulation per data point $(a, b, N, z_{\mathrm{w}}, T)$. Several simulations per data point are required in order to obtain better statistics. That, however, is not feasible. I have used the Multicanonical Chain-Growth Algorithm proposed in [11] in order to simulate a system with the parameter set $(a, b, N, z_{\mathrm{w}})$ and then re-weight to all desired temperatures T.

4.2 Multicanonical Chain-Growth Algorithm

The Multicanonical Chain-Growth Algorithm has been proposed in [11]. The idea is to use the modified weight $W_N = W^{\mathrm{muca}}(E)W^{\mathrm{RR}}$, where E is the energy of the chain. The recursive form of the equation reads:

$$W_n = W_{n-1} m_n \frac{W_n^{\mathrm{muca}}(E_n)}{W_{n-1}^{\mathrm{muca}}(E_{n-1})} \tag{4.8}$$

with $W_0^{\mathrm{muca}} = 1$. Later one can introduce the temperature and re-weight the expected values of all observables to the desired temperature. The key to success lies in the proper choice of the values $W^{\mathrm{muca}}(E)$. A possible way of obtaining these is using an iterative process. One starts with the set of weights $W_n^{\mathrm{muca},(I)}(E) = 1 \quad \forall E, \forall n$, where the superscript I indicates the iteration counter. The first iteration ($I = 1$) with these weights is effectively simulating at infinite temperature $T \to \infty$, i.e. $\beta = 0$. This yields a histogram

$$H_n^{(I)}(E) = \sum_i W_{n,i} \delta_{E,E_i}. \tag{4.9}$$

In the first iteration ($I = 1$) one obtains an estimate of the density of states $\Omega(E)$, i.e. $H_n^{(1)}(E) \propto \Omega_n(E)$. The weights for the next iteration are updated according to the rule

$$W_n^{\mathrm{muca},(I)} = \frac{W_n^{\mathrm{muca}(I-1)}}{H_n^{(I-1)}(E)}. \tag{4.10}$$

After updating the weights, one starts the new iteration, simulating with the those weights. A reasonable guess for the weights has been obtained after several simulations. Following this, a production run can be started where one measures all observables of interest. Obtaining the expectation value of an observable from the production run is done as follows

$$\langle \mathcal{O} \rangle = \frac{\sum_i \mathcal{O}_i W_i \Omega(E_i) e^{-\beta E_i}}{\sum_i W_i \Omega(E_i) e^{-\beta E_i}} \tag{4.11}$$

where $\Omega(E) = H(E)/W^{\mathrm{muca}}(E)$ is the estimate of the density of states up to a multiplicative constant. In practise the iteration in equation 4.11 takes a considerable amount of time, since one iterates over all the output data for every value of β. The formula can be rewritten with sums over the energy values:

$$\langle \mathcal{O} \rangle = \frac{\sum_E H_{\mathcal{O}}(E) \Omega(E) e^{-\beta E}}{\sum_E H(E) \Omega(E) e^{-\beta E}} \tag{4.12}$$

with:

$$H_{\mathcal{O}}(E) = \sum_i \mathcal{O}_i W_i \delta_{E,E_i} \tag{4.13}$$

which saves computational effort.

4.3 Simulations of a free chain

The multicanonical chain-growth algorithm has been used to verify some of the observables obtained from the method of exact enumeration. The results coincide with the exact enumeration and this increases the confidence in the correctness of the data obtained using both methods. Due to the time constraint on the master thesis, further simulations and a systematic analysis of the results could not be performed. However, I will mention some of the problems observed.

The quality of the results from the production run depend highly on the guess for the weights $W^{\text{muca}}(E)$. The quality of the latter however, seems to depend on the fluctuations of the low-energy parts of the histograms $H^(I)(E)$. The more the histograms of the last few iterations fluctuate, the greater the deviation of the data from the production run is from the exact enumeration.

The quality of the results depends even strongly on the choice of the constants $c^>$ and $c^<$. Bad choices deliver completely wrong results with enormous error bars. This is in contrast to most Markov-Chain Monte Carlo simulation methods, where the only parameter that one tunes is usually the temperature.

The error bars obtained with the standard Jackknife method seemed too small for the deviation from the data of the exact enumeration. Several runs using the same set of weights $W^{\text{muca}}(E)$ but different random number sets delivered data that was fluctuating more. Computing the error bars from several runs seems a more reliable method for expressing the confidence intervals.

Further detailed and systematic simulations with longer chains or with the wall constraints could not be performed due to time constraints, therefore no results are provided in this section. Moreover, this part of the study of the system considered in the present work is to be left as a further research opportunity.

Chapter 5

Summary and outlook

The goal of this work was to study the adsorption of polymers onto a stripe-patterned surface. An ISAW was used to model the polymer on a square cubic lattice. The energy of the system was defined as $E(n_\mathrm{s}, n_\mathrm{str}, n_\mathrm{m}) = -\epsilon_\mathrm{s}\left(n_\mathrm{s} + a n_\mathrm{str} + b n_\mathrm{m}\right)$. Varying the monomer-stripe interaction strength via the parameter a allowed for the study of the pattern effects on the behaviour of the system. The phase diagrams obtained show the expected general structure implied from the existing literature. However, the set of available phases depends strongly on the strength of the self-interaction. The latter shifts the collapse transition of the desorbed chain to lower or higher temperatures. Thus the chain can first undergo a collapse transition before it attaches to the surface as a globule or it can undergo collapse after attaching to the surface and form compact conformations at low temperatures. The existence of the "DC" phase is determined bu the relative position of the collapse transition to the position of the adsorption transition. Moreover, the strength of the self-interaction b was not found to affect much the position of the adsorption transition. However, a larger values of b shift the recognition transition to larger values of a as expected.

One of the main differences between long and short chains is that the collapse transition of longer chains moves to higher temperatures and the freezing transition stays approximately at a constant temperature (ignoring artifacts from the choice of the lattice). This increases the temperature range between both transition for larger chains and allows for the existence of a variety of phases when one considers complex systems incorporating an ISAW. Thus, the main disadvantage of the short chains that were used in this work is that both transitions are relatively close to each other in temperature and the temperature of the collapse transition lies below the adsorption transition for equal strengths of all interactions ($a = b = 1$). Moreover, moving the collapse transition to a temperature higher than the adsorption transi-

tion also shifts the freezing transition to higher temperatures. This creates a qualitatively different phase diagram if one wants to compare the results with other studies of similar systems using other lattices and chain lengths. However, the general structure of the phase diagram is similar. This was confirmed by comparing the results of this work with results from a similar off-lattice model.

Moreover, the influence of the stripe width w on the phase diagram was also studied. The existence of a new sub-phase of the recognised phase was found for $w = 2$. The connection of this sub-phase to the freezing transition was established as its position depends only on the strength of the self-interaction b and is approximately equal to the position of the freezing transition. This behaviour is similar to the one found in the reference literature for an off-lattice model [12].

I found that the dependence of the adsorption transition on the system volume, i.e. the distance z_w between the steric and the attractive walls, is significant for distances $z_\mathrm{w} \approx O(N)$ and decreasing for larger z_w. The temperature of the adsorption transition for small values of a was found to be above the temperature of the recognition transition, though for large values of a both merge. The position of the adsorption transition in the regime of small a where no merge with the recognition transition has occurred could be approximated using the formula $T \approx c_1/(c_2 + \log(z_\mathrm{w} + c_3))$, where c_1, c_2 and c_3 are constants. The simulation data yielded a good fit for this equation. The equation is also consistent with a mean-field approximation found in [12], however the c_3 term is relevant on this length scale and cannot be ignored, i.e. a the data does not fit well with $c_3 = 0$.

The position of the recognition transition was found to depend strongly on the strength of the self-attraction. For larger stripe attraction strengths, the dependence of the adsorption and recognition transition temperatures is approximately almost linear, which is expected.

This work used the method of microcanonical analysis as a complementary tool to the canonical analysis for studying the properties of the polymer adsorption. The phase diagrams obtained from the microcanonical method agree with the canonical ones within the uncertainty yielded by the finite size effects. The latter manifest themselves by yielding peaks in the temperature derivatives of canonical expectation values of different observables. These peaks do not appear at the same temperature in the vicinity of a phase transition, but deviate from each other. This can be seen as different lines in the phase diagram which, when bundled together mark the phase transition boundary. This is in contrast to the microcanonical method, which yields (in most cases) only one curve per phase transition. The latter could also be analytically calculated in the trivial cases.

Complementary to the exact enumeration, Monte Carlo simulations using PERM were done in order to save and later visualise relevant conformations. It turned out to be quite easy to obtain conformations knowing, for instance, the energy of those dominating a certain phase. A multicanonical version of the algorithm was also used to verify some of the results from the exact enumeration. The great amount of data produced by the latter took a significant amount of time. Due to the time constraint on the master thesis, this however, did not allow for the study of longer chains using the multicanonical version of PERM. Applying the latter method to the investigated system is left open as an opportunity for further research, since lattice models are easy to simulate and offer an easy way to study finite size scaling.

Chapter 6

Acknowledgement

Finally, I would like to thank Prof. Dr. Wolfhard Janke for giving me the chance to work on this interesting topic and for being very responsive to all of my questions and problems during my work on this thesis. I would also like to thank Prof. Dr. Ulrich Behn for being my second referee and having the time and desire to read and rate my work.

Furthermore, I would like to thank Monika Möddel for supervising my work from the very beginning, for sharing data and knowledge with me, for the helpful discussions, for the patience, as well as for helping me with the correction of mistakes in this thesis.

I am also greatly indebted to Johannes Zierenberg, who also helped me with the correction of this work. Moreover, I would also like to thank all the members of the CQT research group at the Institute of Theoretical Physics at Universität Leipzig for the nice working atmosphere, as well as for the many helpful discussions.

Rüdiger Kürsten, Martin Treffkorn and all the other kicker buddies for the pleasant time playing kicker during the lunch breaks and for the useful discussions relating different fields of physics, as well as everything else.

Last, but not least, I would like to thank my family for being there for me and for supporting me, and of course all the people who have invested lots and lots of hours through the years doing experimental and theoretical research, thus creating the solid scientific foundation on which my work is based.

Bibliography

[1] Nikolai Severin, Jörg Barner, Alexey A. Kalachev, and Jürgen P. Rabe. Manipulation and overstretching of genes on solid substrates. *Nano Letters*, 4(4):577–579, 2004.

[2] Antoine Pallandre, Benoit De Meersman, Françoise Blondeau, Bernard Nysten, and Alain M. Jonas. Tuning the orientation of an antigen by adsorption onto nanostriped templates. *Journal of the American Chemical Society*, 127(12):4320, 2005.

[3] Linda Sawyer, David T. Grubb, and Gregory F. Meyers. *Polymer Microscopy*. Springer, 2008.

[4] Tobias Pirzer and Thorsten Hugel. Adsorption mechanism of polypeptides and their location at hydrophobic interfaces. *ChemPhysChem*, 10(16):2795, 2009.

[5] Carlos Bustamante, Zev Bryant, and Steven B. Smith. Ten years of tension: single-molecule dna mechanics. *Nature*, 421:423, 2003.

[6] Marshall N. Rosenbluth and Arianna W. Rosenbluth. Monte carlo calculation of the average extension of molecular chains. *J. Chem. Phys*, 23(2):356, 1955.

[7] Bernd A. Berg and Thomas Neuhaus. Multicanonical algorithms for first order phase transitions. *Physics Letters B*, 267(2):249 – 253, 1991.

[8] P Grassberger. Monte carlo simulation of 3d self-avoiding walks. *J. Phys. A: Math. Gen.*, 26(12):2769, 1993.

[9] Wolfhard Janke. Multicanonical monte carlo simulations. *Physica A: Statistical Mechanics and its Applications*, 254(1–2):164 – 178, 1998.

[10] Tereza Vrbová and Karel Procházka. Adsorption of self-avoiding walks at an impenetrable plane in the expanded phase: a monte carlo study. *J. Phys. A: Math. Gen.*, 32(29):5469, 1999.

[11] Michael Bachmann and Wolfhard Janke. Multicanonical chain-growth algorithm. *Phys. Rev. Lett.*, 91:208105, 2003.

[12] Monika Möddel. *Statistical Equilibrium Behaviour of Finite Polymers Near Attractive Substrates*. PhD thesis, Universität Leipzig, 2012.

[13] Michael Bachmann and Wolfhard Janke. Substrate adhesion of a non-grafted flexible polymer in a cavity. *Phys. Rev. E*, 73(4):041802, 2006.

[14] Carlo Vanderzande. *Lattice models of polymers*. Cambridge University Press, 1998.

[15] Tereza Vrbová and Stuart G Whittington. Adsorption and collapse of self-avoiding walks and polygons in three dimensions. *J. Phys. A: Math. Gen.*, 29(19):6253, 1996.

[16] Tereza Vrbová and Stuart G Whittington. Adsorption and collapse of self-avoiding walks in three dimensions: A monte carlo study. *J. Phys. A: Math. Gen.*, 31(17):3989, 1998.

[17] Yashwant Singh, Sanjay Kumar, and Debaprasad Giri. Surface adsorption and collapse transition of a linear polymer chain in three dimensions. *J. Phys. A: Math. Gen.*, 32(36):L407, 1999.

[18] Monika Möddel, Michael Bachmann, and Wolfhard Janke. Conformational mechanics of polymer adsorption transitions at attractive substrates. *J. Phys. Chem. B*, 113(11):3314–3323, 2009. PMID: 19231881.

[19] Monika Moddel, Wolfhard Janke, and Michael Bachmann. Systematic microcanonical analyses of polymer adsorption transitions. *Phys. Chem. Chem. Phys.*, 12:11548–11554, 2010.

[20] D MacDonald, S Joseph, D L Hunter, L L Moseley, N Jan, and A J Guttmann. Self-avoiding walks on the simple cubic lattice. *J. Phys. A: Math. Gen.*, 33(34):5973, 2000.

[21] Thomas Vogel, Michael Bachmann, and Wolfhard Janke. Freezing and collapse of flexible polymers on regular lattices in three dimensions. *Phys. Rev. E*, 76:061803, 2007.

[22] Dieter H. E. Gross. *Microcanonical thermodynamics*, volume 66 of *World Scientific Lecture Notes in Physics*. World Scientific Publishing Co. Inc., River Edge, NJ, 2001.

[23] Kurt Kremer and Kurt Binder. Monte carlo simulation of lattice models for macromolecules. *Computer Physics reports*, 7(6):259 – 310, 1988.

[24] Neal Madras and Alan D. Sokal. The pivot algorithm: A highly efficient monte carlo method for the self-avoiding walk. *Journal of Statistical Physics*, 50:109–186, 1988. 10.1007/BF01022990.

[25] Alan D. Sokal. Monte carlo methods for the self-avoiding walk. *Nuclear Physics B - Proceedings Supplements*, 47(1–3):172 – 179, 1996.

[26] F. T. Wall and J. J. Erpenbeck. New method for the statistical computation of polymer dimensions. *J. Chem. Phys*, 30(3):634, 1959.

[27] Peter Grassberger. Pruned-enriched rosenbluth method: Simulations of θ polymers of chain length up to 1 000 000. *Phys. Rev. E*, 56(3):3682, Sep 1997.

[28] Peter Grassberger and Walter Nadler. "go with the winners"-simulations. *eprint arXiv:cond-mat/0010265*, 2000.

[29] Hsiao-Ping Hsu, Vishal Mehra, Walter Nadler, and Peter Grassberger. Growth algorithms for lattice heteropolymers at low temperatures. *J. Chem. Phys*, 118(1):444, 2003.

[30] Thomas Prellberg and Jarosław Krawczyk. Flat histogram version of the pruned and enriched rosenbluth method. *Phys. Rev. Lett.*, 92:120602, 2004.

Appendix A

Exact Enumeration

A.1 Microcanonical scaling of the adsorption transition

A.1.1 $N = 15, b = 1, w = 1, d = 5$

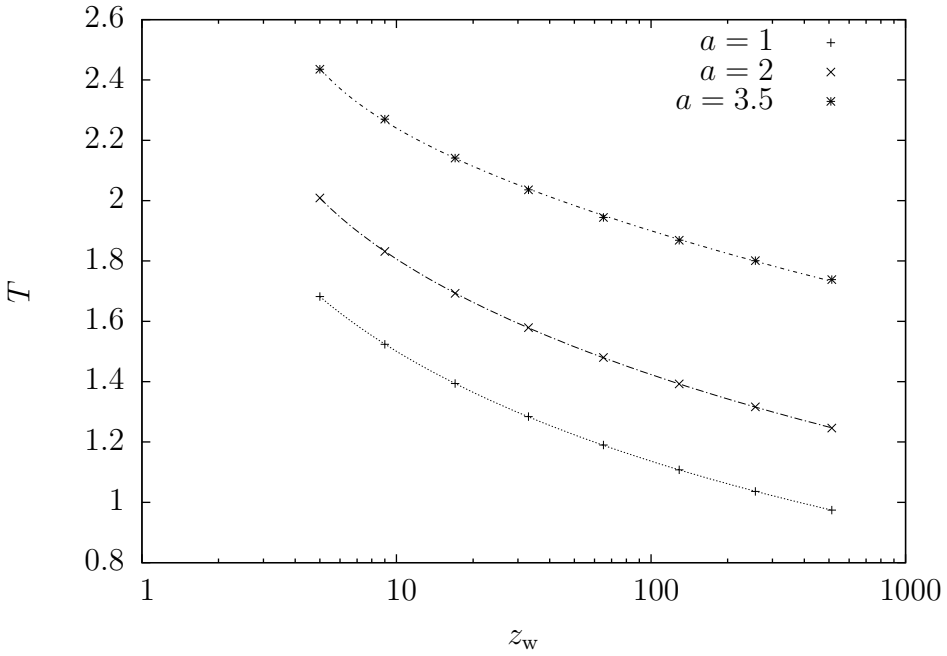

Figure A.1: Fit of the temperature of the adsorption transition in dependance on z_w. The transition temperatures for different values of a have been fitted. Parametrisation $N = 15, b = 1, w = 2, d = 5, z_w = 2^k N + 1$, with $k = 1, 2, \ldots, 8$.

Table A.1: Fit parameteres for equation 3.8 plotted in Figure A.1.

a	c_1	c_2	c_3	error c_1	error c_2	error c_3
1	11.2112	5.2686	-0.955977	0.02735	0.02341	0.0354
2	16.6138	7.08372	-1.7206	0.03639	0.02491	0.0277
3.5	32.53	12.5421	-2.76518	0.5408	0.2792	0.164

Statement of Authorship

I hereby certify that this thesis has been composed by myself, and describes my own work, unless otherwise acknowledged in the text. All references and verbatim extracts have been quoted, and all sources of information have been specifically acknowledged. It has not been accepted in any previous application for a degree.

Momchil Ivanov

After positive appraisal of this thesis, I agree that one copy of my presented thesis may remain at the disposal of the library of Leipzig University.

Momchil Ivanov